

1 **Robustness of epithelial sealing is an emerging property of local ERK** 2 **feedbacks driven by cell elimination**

3 Léo Valon¹, Florence Levillayer¹, Anđela Davidović², Mathilde Chouly¹, Fabiana
4 Cerqueira-Campos¹ and Romain Levayer^{1*}

5 1. Department of Developmental and Stem Cell Biology, Institut Pasteur, CNRS UMR
6 3738, 25 rue du Dr. Roux, 75015 Paris

7 2. Department of Computational Biology, Institut Pasteur, CNRS USR 3756, 28 rue du
8 Dr. Roux, 75015 Paris

9 * Lead contact: romain.levayer@pasteur.fr

10 **Abstract:**

11 **While the pathways regulating apoptosis and cell extrusion are rather well**
12 **described^{1,2}, what regulates the precise spatio-temporal distribution of cell**
13 **elimination in tissues remains largely unknown. This is particularly relevant for**
14 **epithelia with high rates of cell elimination, a widespread situation during**
15 **embryogenesis³⁻⁶ and homeostasis⁷, where concomitant death of neighbours could**
16 **impair the maintenance of epithelial sealing. However, the extent to which epithelial**
17 **tissues can cope with concomitant cell death, and whether any mechanism**
18 **regulates such occurrence have never been explored so far. Here, using the**
19 ***Drosophila* pupal notum (a single layer epithelium) and a new optogenetic tool to**
20 **trigger caspase activation and cell extrusion, we first show that concomitant death**
21 **of clusters of at least three cells is sufficient to transiently impair epithelial sealing.**
22 **Such clustered extrusion was almost never observed *in vivo*, suggesting the**
23 **existence of a mechanism preventing concomitant elimination of neighbours.**
24 **Statistical analysis of cell death distribution in the notum highlighted a transient**
25 **and local protective phase occurring near every dying cell. This protection is driven**
26 **by a transient activation of ERK in the direct neighbours of extruding cells which**
27 **reverts caspase activation and prevents elimination of cells in clusters. Altogether,**
28 **this study demonstrates that the distribution of cell elimination in epithelia is an**
29 **emerging property of transient and local feedbacks through ERK activation which**

30 **is required to maintain epithelial sealing in conditions of high rate of cell**
31 **elimination.**

32 Epithelial cell elimination is driven by extrusion, a succession of remodeling steps
33 removing one cell from the epithelial layer while maintaining epithelial sealing^{1,8}. We first
34 asked whether concomitant extrusion of several neighbours impairs the maintenance of
35 epithelial sealing. As such, we developed a UAS-optoDronc *Drosophila* line, which can
36 trigger rapid caspase activation through blue light-induced clustering of Caspase9
37 (**Figure 1a, Figure S1a**). Expression of optoDronc in fly eyes (GMR-gal4 eye-specific
38 driver) is sufficient to trigger cell death upon blue light exposure and can be rescued by
39 expression of the downstream effector caspase inhibitor p35 (**Figure S1b**). We then used
40 the *Drosophila* pupal notum to assess the efficiency of the construct in triggering epithelial
41 cell elimination. Blue light exposure of clones expressing optoDronc triggers elimination
42 of the majority of cells in less than one hour (**Figure 1b, Figure S1c,e, movie S1**).
43 OptoDronc-triggered extrusions are similar to physiological extrusions in the pupal notum,
44 albeit slightly faster (**Figure S1f**), and require effector caspase activation (**Figure S1d,e,**
45 **movie S1**) like physiological extrusions in the notum^{9,10}. We then induced concomitant
46 elimination of group of cells of various sizes and shapes by expressing optoDronc in
47 clones. While extrusions of single cells or several cells in lines occurred normally (**Figure**
48 **1b,e,f, movie S2 left**), concomitant extrusion of three cells or more in cluster led to
49 aberrant extrusion: cells initiate contraction then relax transiently (**Figure 1c-f, movie S2**
50 **right**) and eventually close the gap through a process akin to wound healing (**Figure 1c,**
51 **E-cad accumulation at vertices, movie S2 right**). Aberrant extrusions correlated with
52 transient flow of injected extracellular fluorescent Dextran in between cells at the level of
53 adherens junctions (**Figure 1g,i,j, movie S3 bottom**), suggesting that epithelial sealing
54 is transiently impaired. Dextran flow however was not observed for cells eliminated in
55 lines (**Figure 1g,h,j, movie S3 top**). Altogether, we conclude that concomitant extrusion
56 (<30 min) of three cells or more in cluster leads to transient loss of epithelial sealing and
57 is thus detrimental for the tissue.

58 Given the rate of cell elimination and assuming that cell eliminations are independent
59 (Poisson process), concomitant elimination of 3 cells or more in cluster should occur

60 several times per movie (See **Methods** for details, more than 2 events per movie of 20
61 hours). Yet, we very rarely observed such clusters during notum morphogenesis (<1 case
62 per movie, **Figure 4j**, n=5 pupae). We therefore checked whether cell death distribution
63 was indeed following locally a Poisson process in the pupal notum. We focused on the
64 posterior region of the notum where cell death distribution is rather uniform in time and
65 space (**Figure 2A**, **movie S4**) to neglect as much as possible the impact of tissue
66 patterning on the rate of cell elimination. We first characterised the distribution of cell
67 death by calculating for every cell elimination the local density of cell death at different
68 distances and different times from the eliminated cell (**Figure 2b**). We obtained a map of
69 local death density for every movie (**Figure 2c**) which was then compared to 200
70 simulations of the death distribution assuming a Poisson process at the same rate of cell
71 elimination. The difference between the simulated map and experimental map was then
72 used to check local differences in the distribution (**Figure 2c**, **Figure S2a**) and averaged
73 for 5 nota (**Figure 2d**). Strikingly, there was in our experimental data a significant
74 reduction in the density of cell elimination in the vicinity of each dying cell (<7 μ m) in a
75 short time window (starting at 10 minutes and up to 60 minutes) compared to the
76 simulated distributions. This suggests that cell death distribution in the posterior region of
77 the pupal notum does not strictly follow a Poisson process, and that a transient (~one
78 hour) and local (~one cell diameter) refractory phase appears in vicinity of each dying
79 cell. To confirm this bias, we then used a closest neighbour analysis (**Figure 2e**): for each
80 cell elimination we detected the nearest elimination in different time windows. While the
81 distribution in late time windows overlapped (1h20' to 2h20', 2h20' to 3h20' after cell death
82 **Figure 2 f,g**), there was a significant decrease of the probability of cell death for the first
83 60 minutes (20 to 80 minutes) following each cell elimination at a distance of 0-10 μ m
84 (~one cell diameter, two folds reduction, p=0.008 for distances<5 μ m). Altogether, we
85 concluded that cell elimination is followed by a transient and local refractory phase (~one
86 cell distance, with a delay of ~10-20 minutes and lasting ~60 minutes) that reduces
87 locally and transiently the probability of cell death (up to 2 folds).

88 These results suggest the existence of active mechanisms preventing the elimination of
89 the neighbours and generating this refractory phase. Effector caspase activation
90 systematically precedes and is required for every cell extrusion in the pupal notum^{9,10}.

91 We therefore tracked caspase dynamics using a GFP live sensor of effector caspase
92 activity (GC3Ai, ^{11,12}) and used the rate of GFP signal accumulation as a proxy for
93 caspase activity (see **Methods**). We frequently observed neighbours simultaneously
94 activating caspases (**Figure 3a, movie S5**), however extrusion of the first cell led to
95 reversion of caspase activity in the neighbours which then remained in the tissue (**Figure**
96 **3a,b,c**, caspase activity goes back to basal levels in the neighbours). This suggested that
97 cell extrusion could inhibit caspase activity and elimination of the direct cell neighbours.
98 We next asked which mechanism could modulate the dynamics of caspase activation and
99 bias the distribution of cell elimination. Recently we showed that the EGFR/ERK pathway
100 is a central regulator of cell elimination and caspase activity in the pupal notum¹⁰, mostly
101 through the inhibition of the pro-apoptotic gene *hid*^{10,13,14}. Moreover, EGFR/ERK can be
102 activated by tissue stretching and downregulated by tissue compaction¹⁰. Using a live
103 sensor of ERK (miniCic-mScarlet, adapted from¹⁰, nuclear accumulation of mScarlet at
104 low ERK activity and nuclear exclusion at high ERK activity, **Figure 3d**), we monitored
105 ERK dynamics near extruding cells. Strikingly, we observed systematically a transient
106 activation of ERK in the direct neighbours of every dying cell (**Figure 3d,f, movie S6,**
107 **Figure S3a,b, movie S7**, activation also observed with EKAR, a ERK FRET sensor¹⁵).
108 This activation was concomitant with the transient stretching of the neighbouring cells
109 triggered by cell extrusion (**Figure 3 e,f**), lasted for ~ 60min and was restricted to the
110 direct neighbours of the dying cell (**Figure 3f**). ERK activation does not correlate with
111 pulses of Calcium (**Figure S4a,b, movie S8**), does not require active secretion of
112 EGF/Spitz from the dying cells (**Figure S4c,d, movie S9**, contrary to enterocytes
113 elimination in the fly midgut¹⁶) and can be mimicked by laser induced cell elimination
114 (**Figure S4e,f, movie S10**). We previously showed that stretch-induced survival in the
115 notum required EGFR¹⁰. Accordingly, ERK activation near dying cells is completely
116 abolished upon EGFR depletion in the tissue (**Figure 3g,h, movie S11**, RNAi previously
117 validated¹⁰). Moreover, EGFR is only required in the neighbouring cells and not in the
118 dying cell (**Figure S3e**). Altogether, this suggested that ERK activation could be driven
119 by the stretching induced by cell extrusion through EGFR activation, although at this stage
120 we cannot exclude other contact dependent mechanisms. Importantly, these pulses of

121 ERK are not restricted to the pupal notum as similar dynamics were observed near dying
122 larval accessory cells in the pupal abdomen (**Figure S3 c,d, movie S12**).

123 We then asked whether ERK pulses were indeed required for caspase reversion in the
124 neighbours. We first correlated ERK dynamics with caspase activity. We observed a
125 significant positive correlation between ERK activity and caspase inhibition with an
126 averaged lag-time of 15 minutes (**Figure 4a-c, movie S13** cross-correlation between
127 nuclear miniCic and GC3Ai differential, $r^2=0.37$). Moreover, caspase reversion in the
128 neighbouring cells was abolished upon EGFR depletion (**Figure 4d-f, movie S14**). Thus,
129 ERK pulses precede and are required for caspase inhibition in the neighbouring cells
130 following each cell death. The localisation and duration of ERK activation (1 row of cells,
131 ~one hour, **Figure 3f**) and the delay with caspases inhibition (15 minutes) were strikingly
132 similar to the death refractory zone we observed near every cell elimination ($<7\mu\text{m}$, 10-
133 20 minutes delay, duration of 60 minutes, **Figure 2**). We therefore checked whether ERK
134 pulses could modulate the spatiotemporal distribution of cell elimination in the posterior
135 region of the notum. Notably, the refractory phase we found in WT pupae (**Figure 2**) was
136 not observed in EGFR depleted nota either using the local density of cell death compared
137 to simulations (**Figure 4g,h, movie S15**), or using the closest neighbours analysis
138 (**Figure 4i**). This suggested that EGFR and ERK pulses are indeed required to generate
139 the transient and local death refractory phase. In absence of local inhibition, we expected
140 to observe spontaneous occurrence of clusters of cell elimination. Accordingly, we
141 observed frequent concomitant extrusion of clusters of cells upon EGFR depletion in the
142 notum (**Figure 4j, movie S16**, >3 cells, ~ 4 events per movie, $n=9$ pupae). These clusters
143 undergo abortive extrusion, transient relaxation followed by wound healing (**Figure 4k,l,**
144 **movie S16**, E-cad accumulation at vertices), similar to the abortive extrusions triggered
145 by optoDronc cell clusters (**Figure 1c-f, movie S2**). Altogether, this showed that ERK
146 pulses are required to reverse caspase activation near dying cells and to prevent
147 elimination of cells in clusters. This feedback is essential to maintain epithelial sealing in
148 conditions with a high rate of cell elimination (**Figure 4m**).

149 High rates of cell elimination are widespread during development and in adult tissues with
150 high cell turnover. Similar local feedbacks mechanisms may be required for coherent cell

151 elimination in the gut to prevent transient and recurrent sealing defects that could lead to
152 chronic inflammation and inflammatory bowel disease¹⁷. Importantly, the mechanism we
153 characterised in this study are conserved in mammals as similar ERK dynamics were
154 observed near dying MCF10A cells which also generate transient resistance to apoptosis
155 (personal communication, Olivier Pertz lab). Interestingly, other reports also described
156 Ca²⁺ and ERK activation waves emanating from extruding MDCK pretumoral cells or
157 caspase-induced MDCK extrusion^{18,19}. However in these cases the waves rather promote
158 extrusion of the dying/extruding cells through collective convergent movements. In
159 contrast, we still see a high rate of cell extrusion upon depletion of ERK feedbacks in our
160 tissue (*UAS-EGFR dsRNA*). Strikingly, the range of the communication seems to be very
161 different between the notum (one cell row) and MDCK cells (10 to 15 cells away),
162 suggesting either that the relays of communication are different, or that mechanical
163 properties of these cells are very different.

164 Although at this stage we cannot rule out the contribution of contact-dependent
165 communication for ERK activation in dying cell neighbours, several evidences point for a
166 contribution of cell stretching. First, ERK activation dynamics correlate very well with
167 transient cell stretching (**Fig. 3e,f**) and occurs very fast (few minutes). Moreover, we
168 previously showed that cell stretching could promote cell survival through EGFR¹⁰.
169 Accordingly, we found that EGFR depletion completely abolished ERK feedbacks near
170 dying cells. We exclude the contribution of calcium signaling or an active secretion of the
171 ligand from the dying cell, while laser induced wound healing was sufficient to promote
172 neighbouring cell stretching and ERK activation. Other recent works have characterized
173 the rapid effect of cell stretching on ERK activation^{20,21}, which was recently shown to also
174 rely on EGFR²². Further work characterising the molecular mechanism of cell deformation
175 sensing by ERK will be required to fully test the contribution of mechanics in extrusion-
176 induced ERK activation.

177 The occurrence of aberrant extrusion strikingly increases for clusters of three cells or
178 more. However, we do not know at this stage what triggers these abnormal extrusions.
179 On the one hand, abortive extrusion may be related to the distance that needs to be
180 closed by the neighbouring cells: while this can be short for lines of cells (using the

181 shortest axis), it will be higher for clusters and may prevent fast fusion of neighbouring
182 cell junctions and gap closure²³. On the other hand, abortive extrusion may be related to
183 caspase-induced remodeling of tricellular junctions²⁴, which are shared by caspase
184 positive cells only in the case of clustered eliminations. Interestingly, some tricellular
185 junction components have been shown to be cleaved by caspases²⁵. Further
186 characterisation of extrusion dynamics will be required to test these hypotheses.

187 Interestingly, 2D simulations of cell disappearance combined with transient death
188 refractory phase in the neighbours suggest that ERK feedbacks could have a strong
189 impact on the total number of dying cells (see **Figure S5a** up to 3 folds reduction for a 60
190 minutes refractory phase, in good agreement with the 2.7 folds increase rate of cell death
191 in the midline upon EGFR depletion¹⁰). Moreover, these feedbacks could be sufficient to
192 increase the rate of cell death near clones resistant to apoptosis provided they are located
193 in regions with a high rate of cell death (see **Figure S5b**, up to 3 folds increase for cells
194 completely surrounded by cells resistant to apoptosis). This suggests that extrusion-
195 driven ERK feedbacks may be sufficient to recapitulate some of the features of cell
196 competition: namely a contact and context dependent increase of cell death near mutant
197 clones²⁶. Altogether, we propose that epithelial robustness and plasticity may be
198 emerging features of local and transient ERK feedbacks driven by cell death.

199 **Acknowledgements**

200 We thank members of RL lab for critical reading of the manuscript, especially Alexis
201 Matamoro-Vidal for suggestions on the manuscript organisation. We would like to thank
202 Jakub Voznica for initiating observations of miniCic in the pupal abdomen during his
203 internship. We also thank Virgile Andreani for help in improving simulations and statistical
204 analysis of the data. We are also grateful to Magalie Suzanne, the Bloomington
205 Drosophila Stock Center, the Drosophila Genetic Resource Center, the Vienna
206 Drosophila Resource Center for sharing stocks and reagents. We also thank B Aigouy for
207 the Packing Analyser software and J. Ellenberg group for MyPic autofocus macro. LV is
208 supported by a Post-doctoral grant “Aide au Retour en France” from the FRM (Fondation
209 pour la Recherche Médicale, ARF20170938651) and a Marie Skłodowska-Curie
210 postdoctoral fellowship (MechDeath, 789573), work in RL lab is supported by the Institut

211 Pasteur (G5 starting package), the ERC starting grant CoSpaDD (Competition for Space
212 in Development and Disease, grant number 758457), the Cercle FSER and the CNRS
213 (UMR 3738).

214 **Authors contribution**

215 RL and LV discussed and designed the project. RL did the experiments with GC3Ai and
216 wrote the manuscript with LV. AD performed the simulations of the theoretical distribution
217 of cell death. FL designed miniCic-Scarlet flies and designed and performed the
218 preliminary test of the optoDronc fly line. MC set up Dextran injection in the pupal notum
219 and initiated experiments with optoDronc. FCC provided the Spitz RNAi movies and part
220 of the WT pupae movies. LV performed all the other analysis and experiments. Every
221 author has commented and edited the manuscript.

222 **Declaration of interests**

223 The authors declare no competing interest

224

225 **Methods**

226 *Drosophila melanogaster* husbandry

227 All the experiments were performed with *Drosophila melanogaster* fly lines with regular
228 husbandry techniques. The fly food used contains agar agar (7.6 g/l), saccharose (53 g/l)
229 dry yeast (48 g/l), maize flour (38.4 g/l), propionic acid (3.8 ml/l), Nipagin 10% (23.9 ml/l)
230 all mixed in one liter of distilled water. Flies were raised at 25°C in plastic vials with a
231 12h/12h dark light cycle at 60% of moisture unless specified in the legends and in the
232 table below (alternatively raised at 18°C or 29°C). Females and males were used without
233 distinction for all the experiments. We did not determine the health/immune status of
234 pupae, adults, embryos and larvae, they were not involved in previous procedures, and
235 they were all drug and test naïve.

236 *Drosophila melanogaster* strains

237 The strains used in this study and their origin are listed in the table below.

Fly line	Chromosome location	Origin (citation)	Source
<i>E-cad-tdTomato (KI)</i>	II	27	BDSC_58789
<i>E-cad-GFP (KI)</i>	II	27	BDSC_60584
<i>UAS-optoDronc</i>	II (attp40)	This study	This study
<i>Tub-miniCic-mScarlet</i>	II	This study	This study
<i>ubi-EKARNls</i>	II	15	Shigeo Hayashi
<i>UAS-EGFR dsRNA</i>	II	VDRC	KK 107130
<i>UAS-spitz dsRNA</i>	II	VDRC	GD 3922
<i>UAS-GcAMPx20</i>	III	Bloomington	BDSC_32236
<i>UAS-GC3Ai</i>	III	11	Magalie Suzanne
<i>GMR-gal4</i>	II	Bloomington	BDSC_1104
<i>UAS-his3.3 mIFP-T2A-H01</i>	III	Bloomington	BDSC_64184
<i>Hs-flp22; ; Act<cd2<gal4,UAS-GFP</i>	I; III	10	10

238

239 The exact genotype used for each experiment is listed in the next table. ACI: time After
240 Clone Induction, APF: After Pupal Formation, n: number of pupae/adults.

Figure	Genotype	Heat shock 37°C	Stage	n
1b-j	<i>hs-flp22; E-cad-tdTomato (KI)/UAS-optoDronc ; act<y+<gal4 , UAS-GFP/+</i>	12 min, 2 days ACI	30h APF	10
2a	<i>E-cad-GFP (KI), tub-miniCic-mScarlet ; pnr-gal4, UAS-His3-mIFP</i>	N/A	16h APF	5
3a-c	<i>E-cad-tdTomato (KI)/+; pnr-gal4/UAS-GC3Ai</i>	N/A	20h APF	3
3d-f	<i>E-cad-GFP (KI), tub-miniCic-mScarlet ; pnr-gal4, UAS-His3-mIFP</i>	N/A	20h APF	5 (quantified on 2)
3g	<i>E-cad-GFP (KI), tub-miniCic-mScarlet/UAS-EGFR dsRNA ; pnr-gal4, UAS-His3-mIFP/+</i>	N/A	16h APF	3 (quantified on 2)
4a-c	<i>tub-miniCic-mScarlet ; pnr-gal4/UAS-GC3Ai</i>	N/A	20h APF	3
4d-f	<i>E-cad-tdTomato (KI)/UAS-EGFR dsRNA; pnr-gal4/UAS-GC3Ai</i>	N/A	20h APF	3
4g-l	<i>E-cad-GFP (KI), tub-miniCic-mScarlet/UAS-EGFR dsRNA ; pnr-gal4, UAS-His3-mIFP/+</i>	N/A	16h APF	9
S1a	<i>E-cad-tdTomato (KI)/UAS-optoDronc; pnr-gal4/+</i>	N/A	16h APF	2
S1b	<i>GMR-gal4/UAS-optoDronc (dark)</i>	N/A	Adult	20
S1b	<i>GMR-gal4/UAS-optoDronc (blue light)</i>	N/A	Adult	19
S1b	<i>GMR-gal4/UAS-optoDronc ; UAS-p35/+ (blue light)</i>	N/A	Adult	46
S1c	<i>hs-flp22; E-cad-tdTomato (KI)/UAS-optoDronc ; act<y+<gal4 , UAS-GFP/+</i>	12 min, 2 days ACI	30h APF	3
S1c	<i>hs-flp22, E-cad-tdTomato (KI)/UAS-optoDronc ; act<y+<gal4 , UAS-GFP/UAS-p35</i>	12 min, 2 days ACI	30h APF	3
S1f	<i>hs-flp22, E-cad-tdTomato (KI)/UAS-optoDronc ; act<y+<gal4 , UAS-GFP/+</i>	12 min, 2 days ACI	30h APF	3
S1f	<i>E-cad-GFP (KI), tub-miniCic-mScarlet ; pnr-gal4, UAS-His3-mIFP</i>	N/A	30h APF	5
S2a	<i>E-cad-GFP (KI), tub-miniCic-mScarlet ; pnr-gal4, UAS-His3-mIFP</i>	N/A	16h APF	5
S2b	<i>E-cad-GFP (KI), tub-miniCic-mScarlet/ UAS-EGFR dsRNA ; pnr-gal4, UAS-His3-mIFP</i>	N/A	16h APF	4
S3a,b	<i>tub-miniCic-mScarlet ; pnr-gal4/ubi-EKARnls</i>	N/A	20h APF	4
S3c,d	<i>E-cad-GFP (KI), tub-miniCic-mScarlet</i>	N/A	abdomen (20h APF)	2
S3e	<i>Hs-flp22; E-cad-GFP (KI), tub-miniCic-mScarlet/UAS-EGFR dsRNA ; act<y+<gal4, UAS-His3-mIFP/+</i>	20 min, 2 days ACI	20h APF	3
S4a,b	<i>E-cad-tdTomato (KI)/+; pnr-gal4/UAS-GCaMPx20</i>	N/A	16h APF	2
S4c,d	<i>Hs-flp22; E-cad-GFP (KI), tub-miniCic-mScarlet/UAS-spitz dsRNA ; act<y+<gal4, UAS-His3-mIFP/+</i>	20 min, 2 days ACI	20h APF	2
S4e,f	<i>E-cad-GFP (KI), tub-miniCic-mScarlet ; pnr-gal4, UAS-His3-mIFP</i>	N/A	20h APF	7

242 Design of optoDronc

243 The GFP-linker-DRONC-linker-CRY2PHR was first cloned in the pCasper4-Tubp-Gal80
244 vector (addgene 17748) and subsequently cloned in the pJFRC4-3XUAS-IVS-
245 mCD8::GFP (Addgene 26217). Initial cloning was performed by three successive
246 amplifications/ligations. Briefly, GFP was first inserted in pCasper4-Tubp by PCR-
247 amplifying GFP from pJFRC19-13XLexAop2-IVS-myr::GFP (Addgene 26224) adding
248 NotI, BglII, XbaI restriction sites and linkers, and eventually ligation into pCasper4-TubP-
249 Gal80 after digestion with NotI and XbaI. Dronc cDNA was then inserted in this plasmid
250 through PCR amplification on the cDNA clone LP09975 (DGRC) adding BglII, NheI and
251 XbaI restriction sites and linkers, and then ligation into pCasper4-TubP-GFP-linker cut
252 with BglII and XbaI. Finally, CRY2PHR was inserted by amplifying residues 1-498 of
253 CRY2 from pGal4BD-CRY2 (Addgene 28243) while adding NheI and XbaI sites and
254 ligation into pCasper4-TubP-GFP-linker-DRONC-linker cut with NheI and XbaI. The GFP-
255 linker-Dronc-linker-CRY2PHR was cut with NotI and XbaI and inserted by ligation in
256 pJFRC4-3XUAS-IVS-mCD8::GFP (Addgene 26217) after digestion with NotI and XbaI.
257 The construct was checked by sequencing and inserted at the attP site attP40A after
258 injection by Bestgene. The primers used for the construct are listed below (restriction sites
259 in bold and linker in italic).

Insert	Forward	Reverse
GFP-linker	TTATAG CGGCCG CATGTCCAAAGGT GAAGAACT	AATTT CTAGAAGATCT <i>GCCGCC</i> TCC TCCGG ACCCACCACCTCCAGAGCCACCGCCACCC TTGTAGAGCTCATCCATGCCGT
DRONC-linker	AATT AGATCT ATGCAGCCGCCGGAG CTCGAGATT	AATTT CTAGAGCTAGC <i>GCCGCC</i> TCC TCCGG ACCCACCACCTCCAGAGCCACCGCCACCT TCGTTGAAAAACCCGGGATTG
CRY2PHR	AATT AGATCT ATGCAGCCGCCGGAG CTCGAGATT	AATTT CTAGACT ATGCTGCTCCGATCATGATCTGT

260

261 Induction of cell death using optoDronc

262 To induce optoDronc in the eye, GMR-gal4 females were crossed with homozygous
263 males UAS-optoDronc. Tubes containing crosses and progeny were either kept in the
264 dark at 25°C (control) or maintained in a cardboard box permanently lighted by a blue

265 LED array (LIU470A, Thorlab) in the same 25° incubator as the control. Female adult
266 eyes were then imaged on a Zeiss stereoV8 binocular equipped with a colour camera
267 (Axiocam Icc5).

268 For induction of optoDronc in clones in the pupal notum, *hs-flp; E-cad-tdTomato(KI);*
269 *act<cd2<G4* females were crossed with homozygous *UAS-optoDronc* or *UAS-optoDronc;*
270 *UAS-p35*. Clones were induced through a 12 minutes heat shock in a 37°C waterbath.
271 Tubes were then maintained in the dark at 25°C. White pupae were collected 48 hours
272 after clone induction and aged for 24h at 25°C in the dark. Collection of pupae and
273 dissection were performed on a binocular with LED covered with home-made red filter
274 (Lee colour filter set, primary red) after checking that blue light was effectively cut (using
275 a spectrometer). Pupae were then imaged on a spinning disc confocal (Gataca system).
276 The full tissue was exposed to blue light using the diode 488 of the spinning disc system
277 (12% AOTF, 200ms exposure per plane, 1 stack/min). The proportion of remaining cells
278 was calculated by measuring the proportion of cells remaining in the tissue at time *t*
279 compared to *t*₀. Extrusion profiles were obtained by segmenting extruding cells in the
280 optoDronc clones with E-cad-tdTomato signal (only single cell clones in this case) or WT
281 cells marked with E-cad-GFP in the posterior region of the notum using Packing
282 analyser²⁸. Curves were aligned on the termination of extrusion (no more apical area
283 visible) and normalised with the averaged area on the first five points. Clone area profile
284 (**Figure 1d, Figure 4I**) were obtained by segmenting the group of cells in the clone and
285 calculating the area and the solidity (Area/Convex Area) on Matlab. Categorisation of
286 normal versus abnormal extrusion was based on the dynamics of clone contraction:
287 transient relaxation or accumulation of E-cad at vertices was counted as abnormal
288 extrusion. Large relaxation combined with clear E-cad accumulation at vertices was
289 counted as “transient holes”.

290 **Design of miniCic-mScarlet**

291 The pCaspaseR4-Tubp-miniCic-linker-mScarlet-I was obtained by amplifying by PCR
292 miniCic-linker from pCaspaseR4-Tubp-miniCic-linker-mCherry¹⁰ and mScarlet-I from
293 pmScarlet-i_C1 (Addgene 85044). These two inserts were cloned in the vector
294 pCaspaseR4-TubP-Gal80 linearised by NotI, XbaI digestion (to excise Gal80) using

295 NEBuilder HiFi DNA Assembly Method. The construct was checked by sequencing and
296 inserted through P-element after injection by Bestgene. The primers used for the
297 construct are listed below.

Insert	Forward	Reverse
miniCic-linker	GTGAAGGTACCCGCCCGGGGATCAGATCC	ACAGAACCACCACCAGAACCAC
mScarlet-i	CGGTGGTGGTTCTGGTGGTGGTTCTGTGAGCAAGGGC GAGGCA	CAGAAGTAAGTTCTTCACAAAGATCCTCTAGATTACTTGTACAGCTC GTCCATGC

298

299 The construct was tested by comparing the dynamics and pattern in the notum compared
300 to previously characterised dynamics using miniCic-mCherry¹⁰. Similar dynamics were
301 also observed at the single cell level between miniCic-mScarlet and the FRET sensor ubi-
302 EKARnls¹⁵ (**Fig. S3**).

303 **Live imaging and movie preparation**

304 Notum live imaging was performed as followed: the pupae were collected at the white
305 stage (0 hour after pupal formation), aged at 29°, glued on double sided tape on a slide
306 and surrounded by two home-made steel spacers (thickness: 0.64 mm, width 20x20mm).
307 The pupal case was opened up to the abdomen using forceps and mounted with a
308 20x40mm #1.5 coverslip where we buttered halocarbon oil 10S. The coverslip was then
309 attached to spacers and the slide with two pieces of tape. Pupae were collected 48 or
310 72h after clone induction and dissected usually at 16 to 18 hours APF (after pupal
311 formation). The time of imaging for each experiment is provided in the table above. Pupae
312 were dissected and imaged on a confocal spinning disc microscope (Gataca systems)
313 with a 40X oil objective (Nikon plan fluor, N.A. 1.30) or 100X oil objective (Nikon plan fluor
314 A N.A. 1.30) or a LSM880 equipped with a fast Airyscan using an oil 40X objective (N.A.
315 1.3), Z-stacks (1 µm/slice), every 5min using autofocus at 25°C. The autofocus was
316 performed using E-cad-GFP plane as a reference (using a Zen Macro developed by Jan
317 Ellenberg laboratory, MyPic) or a custom made Metamorph journal on the spinning disc.
318 Movies were performed in the nota close to the scutellum region containing the midline
319 and the aDC and pDC macrochaetae. Movies shown are adaptive local Z-projections.
320 Briefly, E-cad plane was used as a reference to locate the plane of interest on sub

321 windows (using the maximum in Z of average intensity or the maximum of the standard
322 deviation). Nuclear signal was then obtained by projecting maximum of intensity on 7 μm
323 (7 slides) around a focal point which was located 6 μm basal to adherens junctions (see
324 ¹⁰ for more details).

325 **Laser ablation**

326 Photo-ablation experiments were performed using a pulse UV-laser (355nm, Teem
327 photonics, 20kHz, peak power 0.7kW) coupled to a llas-pulse module (Gataca-systems)
328 attached to our spinning disk microscope. The module was first calibrated and then set
329 to 40-60% laser power. Images were taken every 500ms and 3 to 6 single cells were
330 ablated 10 images after the beginning of the movie (20 repetitions of “point” ablation
331 ~50ms exposure per cell). Cells were selected in regions with high and homogeneous
332 nuclear miniCic levels. For each single cell ablation, miniCic signals over time were
333 extracted in 4 cell nuclei of the first row and second row of cells around the ablated cell.
334 Nuclei were visualized and clicked by hand using the Histone3-mIFP fluorescent channel
335 after a local z-projection. Background value for each movies (for miniCic) were extracted
336 and removed from the signals, then the single cell miniCic signal was normalized to 1
337 using the first time point.

338 **Dextran injection in pupal notum**

339 30h APF pupae were glued on double sided tape and the notum was dissected with red
340 filter. Pupae were then injected using home-made needles (borosilicate glass capillary,
341 outer diameter 1mm, internal diameter 0.5mm, 10cm long, Sutter instruments) pulled with
342 a Sutter instrument P1000 pipette pulling apparatus. Dextran Alexa 647 10,000 MW
343 (Thermofisher, D22914) was injected at 2mg/ml in the thorax of the pupae using a
344 Narishige IM400 injector using a constant pressure differential (continuous leakage) and
345 depressurisation in between pupae. Imaging of Dextran leakage in live pupae was
346 performed after local projection using E-cad plane as a reference to measure Dextran
347 concentration at the junction plane (note that septate junctions are located basally to
348 adherens junctions). Dextran intensity was measured using a ROI in the center of the
349 clone after normalization using the first 5 time points and removal of intensity background

350 (estimated on a region with no signal. Note that Dextran injection cannot be used to track
351 leakages over long time scales (>4 hours) as the majority of Dextran get rapidly trapped
352 in fat body cells and in epithelial cell endosomes.

353 **Signaling dynamics and cross-correlation**

354 *Measurement of ERK activity*

355 ERK dynamics were measured using the mean nuclear intensity of miniCic. Whenever
356 possible, a marker of the nucleus (His3-mIFP) was used to track the nucleus manually
357 (Fiji macro). EKAR FRET signal was obtained after local projection on 6 planes of CFP
358 and YFP signals. CFP and YFP signals were blurred (Gaussian blur, 2 pixel width) and
359 the ratio of YFP/CFP signal was then calculated. Raw YFP-nls signal was thresholded
360 and used as a mask to only keep nuclear FRET signal. For the comparison of miniCic
361 and EKAR, single curves from the same cell were aligned on the peak of the FRET signal
362 (maximum value) and eventually averaged for all the cells.

363 For the measurement of miniCic in neighbours combined with apical area (**Figure 3**), cell
364 contours were tracked using E-cad-GFP (Packing analyser), while nuclei were manually
365 tracked on Matlab using His3-mIFP. For each dying cell, the nuclear miniCic intensity and
366 apical area were averaged for all the neighbours (first row and second row of cells). The
367 final curves are averaged of each of these curves after alignment at the termination of
368 cell extrusion (apical area=0). Note that the “n” used for s.e.m. calculation is not the total
369 number of neighbours, but the number of cell clusters.

370 *Analysis of GC3Ai signal*

371 To analyse caspase activity, we used the differential of GC3Ai signal as a proxy. GC3Ai
372 becomes fluorescent upon cleavage of a domain by effector caspases which triggers GFP
373 folding and maturation¹¹. The dynamics of GFP signal can be written as follows:

$$374 \frac{dG}{dt} = C \cdot G_0 - \alpha \cdot G$$

375 Where G stands for concentration of active GFP, C concentration of active effector
376 caspase, G₀ concentration of inactive GFP, and α rate of GFP degradation.

377 On timescales of one hour, we can neglect GFP degradation. Assuming a constant pool
378 of inactive GC3Ai, G_0 can be considered as a constant. As such:

379
$$\frac{dG}{dt} = C \cdot G_0$$

380 Therefore the change of intensity over time should be proportional to effector caspase
381 activity (C). Practically, GC3Ai signal was obtained after local projection (using E-cad or
382 nuclear miniCic as a reference) and measurement of mean intensity on small circular ROI
383 at the center of the cell (Fiji). The differential was calculated using the Diff function of
384 Matlab after smoothing the intensity curve (10 time points averaging window) and aligning
385 the curve on the time of disappearance (end of extrusion) of the first cell. Note that the
386 analysis of caspase reversion was restricted to neighbours having a positive slope before
387 the elimination of the first cell (in order to see caspase shutdown).

388 To cross-correlate GC3Ai and ERK dynamics, local projections centered on nuclear
389 miniCic were used (with GC3Ai plane of interest shifted apically). miniCic nuclear intensity
390 and GC3Ai cytoplasmic intensity were measured by manually tracking small circular ROI
391 (20px) in the center of the cells (Fiji home-made macro). The cross-correlation between
392 GC3Ai differential and miniCic nuclear signal was calculated on Matlab with the “xcorr”
393 function with the ‘coef’ option (normalised cross-correlation). All the curves (one per cell)
394 were then averaged.

395 *Measurement of GCaMP*

396 GCaMP signal was measured on local projections using E-cad-tdTomato as a reference
397 plane after global correction for bleaching. Each cell extrusion was cropped and the movie
398 realigned using the Stackreg Fiji plugin. GCaMP signal was then measured using the
399 mean intensity in a 20x20 pixel square in the center of each cells. Each single cell curve
400 was aligned (time 0 at the termination of extrusion) and normalised using 5 time values
401 around time 0.

402 **Statistical analysis of cell death distribution**

403 *Calculation of the probability to observe three cells clustered elimination*

404 We wanted to evaluate the probability to observe a cluster of three cells eliminated in less
405 than 30 minutes. We first considered a hexagonal grid of points in a squared array (N
406 cells per side) and assumed periodic boundaries. The probability of cell disappearance
407 over 30 min is p . As such the probability to observe a specific cluster of 3 cells eliminated
408 in the same 30 min window is p^3 . The total number of possible 3 cells configurations is
409 approximatively given by: $2 \cdot N^2$.

410 Using the posterior region of WT nota, we estimate $p \sim 0.04$ (probability of cell elimination
411 in 30 minutes). As such for a group of 400 cells (region of interest used in **Figure 2**)
412 observed for 20 hours ($T = 40$ times 30 minutes), the expected number of 3 cell-cluster
413 elimination is given by: $E(\text{number of clusters}) = 2N^2p^3T = \mathbf{2.05}$.

414 Therefore, we would expect to observe several occurrences of 3 cell-cluster eliminations
415 per movie.

416 *Analysis of death distribution*

417 For the analysis of death distribution we selected movies lasting 16 to 20 hours in the
418 posterior region of the pupal notum. Cell extrusion events were clicked by hand and
419 checked twice. Extrusion localisations were corrected for global drift (translation) of the
420 tissue (Matlab procedure). Spatiotemporal distribution of death was first checked by x-y-
421 t histogram. According to that distribution, for each movie, an area of interest (in time and
422 space) was selected by hand to obtain an area where distribution was as homogeneous
423 as possible (double checked by x-y-t histograms). These data sets were then the basis
424 of two statistical analyses (see below).

425 *1. Determination of the distribution of distances:*

426 All distances in time and space between all extrusions were computed. We then plotted
427 the histogram of density of death at a given distance (number of deaths divided by the
428 area of the disc considered) as a function of spatial and temporal distances from each
429 dying cell. In parallel, we extracted from these data the experimental probability of dying.
430 For each experiment, we ran 200 simulations where we placed randomly the same
431 number of deaths as the experiment in x, y, t (assuming independent events). For each
432 simulation we evaluated all the distances and the histograms of death densities, and

433 calculated the mean of the 200 simulations. Finally, we calculated the differences
434 between histograms of densities from simulations and histograms of the experiments for
435 every single movie. We then used the average of the “difference map” for each
436 experiment (5 for WT, 4 for EGFR-RNAi).

437 *2. Closest neighbour analysis:*

438 For each death event, we calculated the Euclidean distance to the closest death in a given
439 time window. Based on the previous analysis, we selected windows of 20' to 1h20', 1h20'
440 to 2h20' and 2h20' to 3h20'. We excluded the first 20 minutes as they correspond to the
441 characteristic time of extrusion (where cells cannot be reverted anymore). We then sorted
442 these shortest distances by size and plotted the cumulative probability of closest death at
443 a given distance. A value of 40% at a distance of 10 micrometers means that 40% of the
444 closest deaths are localized between 0 and 10 micrometers away.

445 **2D simulations of death rate**

446 To evaluate the effect of the duration of the feedback as a function of the intrinsic
447 probability of dying we ran the following model based on a Matlab routine. Parameters of
448 the model are the following: “n”, number of cells per side, “PN”, probability of a cell to die
449 per time-point, “T”, duration of the inhibition in time-points.

450 Cells are embedded in a hexagonal grid of n-by-n points. The cells can be in 2 different
451 states: “regular” (sensitive to death), or “inhibited for death” (probability to die=0). For
452 each time point, for each regular cell, we get a random value between 0 and 1. If the value
453 is below the dying probability, then the cell will be considered as dying. At the end of the
454 evaluation of every cell, the total number of dying cells is recorded and the neighbours of
455 the dying cell and the dying cell itself are set to “inhibited for cell death” for T time points.
456 For every simulation, we run 1000 time-points and evaluate the mean value of number of
457 deaths per time points in the steady-state regime (obtained after the 500 times). 5
458 simulations were run for all different conditions (with different T values and PN values).

459 **Calculation of death probability with caspase resistant neighbours**

460 Assuming a constitutive rate of cell elimination λ (number of cell death.min⁻¹), a total
461 refractory phase of a duration of T and n the number of caspase resistant neighbours (0
462 to 6). The effective probability for a cell to die per minute is given by the following
463 expression:

$$464 \quad p(n) = \lambda \cdot [(1 - \lambda)^T]^{(6-n)}$$

465 Where $[(1 - \lambda)^T]^{(6-n)}$ gives the probability for not being in a refractory phase (probability
466 that no neighbour died in the last T minutes, excluding the cells resistant for apoptosis
467 which will never die). Note that we neglect here the effect of the n+2 neighbours and
468 assume that all other non-resistant neighbours have the same elimination rate λ .

469 **Statistics**

470 Data were not analysed blindly. No specific method was used to predetermine the number
471 of samples. The definition of n and the number of samples is given in each figure legend
472 and in the table of the Experimental model section. Error bars are standard error of the
473 mean (s.e.m.). p-values are calculated through t-test if the data passed normality test
474 (Shapiro-Wilk test), or Mann-Whitney test/Rank sum test if the distribution was not
475 normal. Statistical tests were performed on Graphpad Prism 8 or Matlab.

476 **References**

- 477 1 Gudipaty, S. A. & Rosenblatt, J. Epithelial cell extrusion: Pathways and pathologies. *Semin Cell Dev Biol*, doi:10.1016/j.semcd.2016.05.010 (2016).
- 479 2 Fuchs, Y. & Steller, H. Programmed cell death in animal development and disease. *Cell* **147**, 742-
480 758, doi:10.1016/j.cell.2011.10.033 (2011).
- 481 3 Toyama, Y., Peralta, X. G., Wells, A. R., Kiehart, D. P. & Edwards, G. S. Apoptotic force and tissue
482 dynamics during *Drosophila* embryogenesis. *Science* **321**, 1683-1686,
483 doi:10.1126/science.1157052 (2008).
- 484 4 Monier, B. *et al.* Apico-basal forces exerted by apoptotic cells drive epithelium folding. *Nature*
485 **518**, 245-248, doi:10.1038/nature14152 (2015).
- 486 5 Ninov, N., Chiarelli, D. A. & Martin-Blanco, E. Extrinsic and intrinsic mechanisms directing
487 epithelial cell sheet replacement during *Drosophila* metamorphosis. *Development* **134**, 367-379,
488 doi:10.1242/dev.02728 (2007).
- 489 6 Marinari, E. *et al.* Live-cell delamination counterbalances epithelial growth to limit tissue
490 overcrowding. *Nature* **484**, 542-545, doi:10.1038/nature10984 (2012).
- 491 7 Williams, J. M. *et al.* Epithelial cell shedding and barrier function: a matter of life and death at the
492 small intestinal villus tip. *Vet Pathol* **52**, 445-455, doi:10.1177/0300985814559404 (2015).

- 493 8 Ohsawa, S., Vaughen, J. & Igaki, T. Cell Extrusion: A Stress-Responsive Force for Good or Evil in
494 Epithelial Homeostasis. *Dev Cell* **44**, 532, doi:10.1016/j.devcel.2018.02.007 (2018).
- 495 9 Levayer, R., Dupont, C. & Moreno, E. Tissue Crowding Induces Caspase-Dependent Competition
496 for Space. *Curr Biol* **26**, 670-677, doi:10.1016/j.cub.2015.12.072 (2016).
- 497 10 Moreno, E., Valon, L., Levillayer, F. & Levayer, R. Competition for Space Induces Cell Elimination
498 through Compaction-Driven ERK Downregulation. *Curr Biol* **29**, 23-34 e28,
499 doi:10.1016/j.cub.2018.11.007 (2019).
- 500 11 Schott, S. *et al.* A fluorescent toolkit for spatiotemporal tracking of apoptotic cells in living
501 *Drosophila* tissues. *Development* **144**, 3840-3846, doi:10.1242/dev.149807 (2017).
- 502 12 Zhang, J. *et al.* Visualization of caspase-3-like activity in cells using a genetically encoded
503 fluorescent biosensor activated by protein cleavage. *Nat Commun* **4**, 2157,
504 doi:10.1038/ncomms3157 (2013).
- 505 13 Kurada, P. & White, K. Ras promotes cell survival in *Drosophila* by downregulating hid expression.
506 *Cell* **95**, 319-329 (1998).
- 507 14 Bergmann, A., Agapite, J., McCall, K. & Steller, H. The *Drosophila* gene hid is a direct molecular
508 target of Ras-dependent survival signaling. *Cell* **95**, 331-341 (1998).
- 509 15 Ogura, Y., Wen, F. L., Sami, M. M., Shibata, T. & Hayashi, S. A Switch-like Activation Relay of EGFR-
510 ERK Signaling Regulates a Wave of Cellular Contractility for Epithelial Invagination. *Dev Cell*,
511 doi:10.1016/j.devcel.2018.06.004 (2018).
- 512 16 Liang, J., Balachandra, S., Ngo, S. & O'Brien, L. E. Feedback regulation of steady-state epithelial
513 turnover and organ size. *Nature* **548**, 588-591, doi:10.1038/nature23678 (2017).
- 514 17 Blander, J. M. Death in the intestinal epithelium-basic biology and implications for inflammatory
515 bowel disease. *FEBS J* **283**, 2720-2730, doi:10.1111/febs.13771 (2016).
- 516 18 Takeuchi, Y. *et al.* Calcium Wave Promotes Cell Extrusion. *Curr Biol*,
517 doi:10.1016/j.cub.2019.11.089 (2020).
- 518 19 Aikin, T. J., Peterson, A. F., Pokrass, M. J., Clark, H. R. & Regot, S. Collective MAPK Signaling
519 Dynamics Coordinates Epithelial Homeostasis. *Bioarchive*, doi:<https://doi.org/10.1101/826917>
520 (2019).
- 521 20 Aoki, K. *et al.* Stochastic ERK activation induced by noise and cell-to-cell propagation regulates cell
522 density-dependent proliferation. *Mol Cell* **52**, 529-540, doi:10.1016/j.molcel.2013.09.015 (2013).
- 523 21 Aoki, K. *et al.* Propagating Wave of ERK Activation Orients Collective Cell Migration. *Dev Cell* **43**,
524 305-317 e305, doi:10.1016/j.devcel.2017.10.016 (2017).
- 525 22 Hino, N. *et al.* ERK-mediated mechanochemical waves direct collective cell polarization.
526 *Bioarchive*, doi:<https://doi.org/10.1101/2019.12.25.888552> (2019).
- 527 23 Staddon, M. F. *et al.* Cooperation of dual modes of cell motility promotes epithelial stress
528 relaxation to accelerate wound healing. *PLoS Comput Biol* **14**, e1006502,
529 doi:10.1371/journal.pcbi.1006502 (2018).
- 530 24 Higashi, T. & Chiba, H. Molecular organization, regulation and function of tricellular junctions.
531 *Biochim Biophys Acta Biomembr* **1862**, 183143, doi:10.1016/j.bbamem.2019.183143 (2020).
- 532 25 Janke, S., Mittag, S., Reiche, J. & Huber, O. Apoptotic Fragmentation of Tricellulin. *Int J Mol Sci* **20**,
533 doi:10.3390/ijms20194882 (2019).
- 534 26 Claveria, C. & Torres, M. Cell Competition: Mechanisms and Physiological Roles. *Annu Rev Cell Dev*
535 *Biol* **32**, 411-439, doi:10.1146/annurev-cellbio-111315-125142 (2016).
- 536 27 Huang, J., Zhou, W., Watson, A. M., Jan, Y. N. & Hong, Y. Efficient ends-out gene targeting in
537 *Drosophila*. *Genetics* **180**, 703-707, doi:10.1534/genetics.108.090563 (2008).
- 538 28 Etournay, R. *et al.* TissueMiner: A multiscale analysis toolkit to quantify how cellular processes
539 create tissue dynamics. *Elife* **5**, doi:10.7554/eLife.14334 (2016).

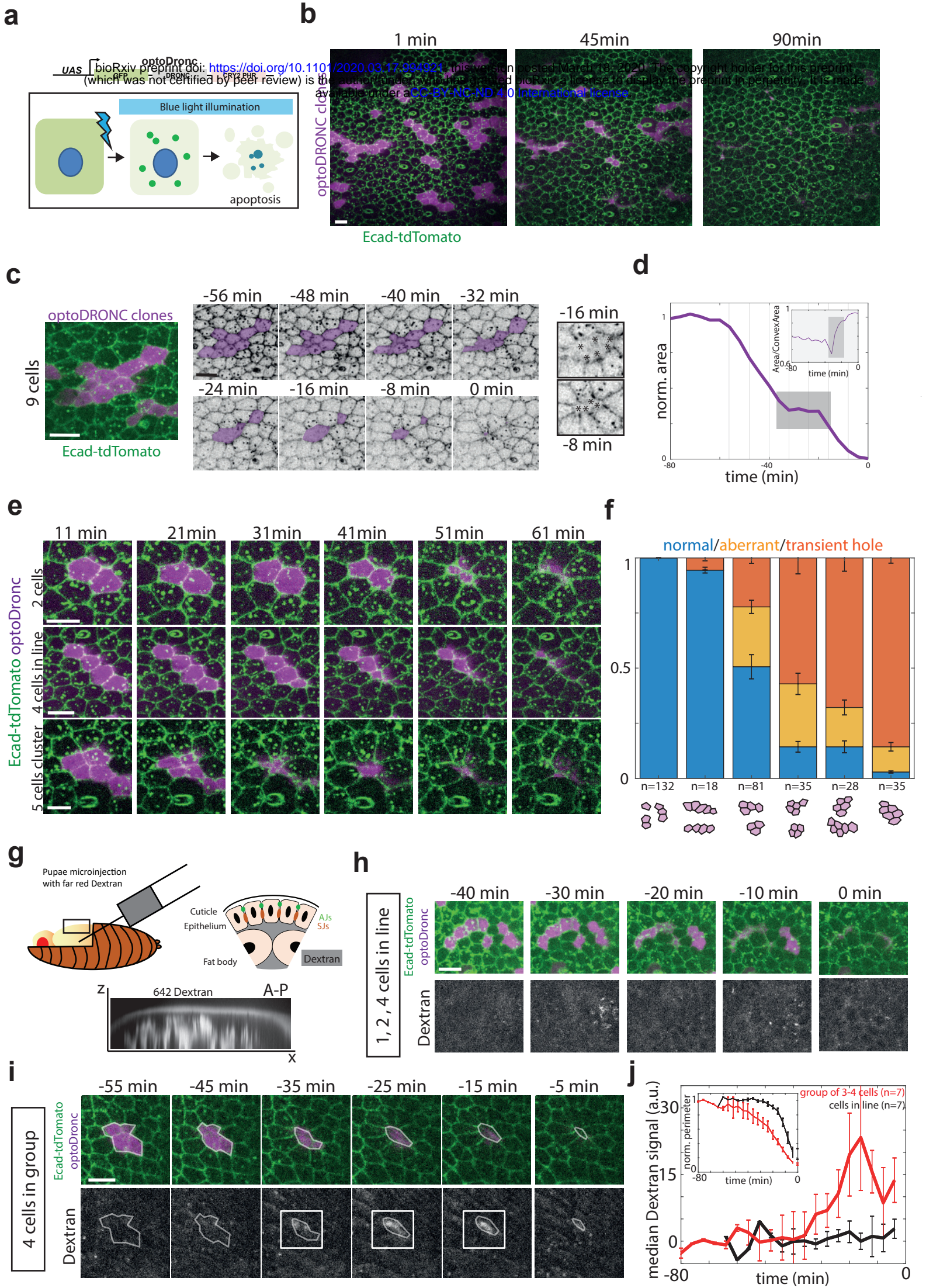


Figure 1: Extrusion of a cluster of more than three cells is sufficient to impair epithelial sealing

a: Schematic of the UAS-optoDronc construct. The cDNA of Dronc (*Drosophila* Caspase9) is fused to eGFP in N-ter and the blue light sensitive protein CRY2-PHR in C-ter. Upon blue light exposure, optoDronc clusterises (green dots) and triggers caspase activation and apoptosis.

b: Snapshots of a live pupal notum expressing optoDronc in clones (magenta, local z-projection) and E-cad-tdTomato. Most of the clones disappear after 60 minutes of blue light exposure. Scale bar= 10 μ m.

c: Elimination of an optoDronc clone of nine cells. Snapshots of inverted E-cad-tdTomato signal. Time 0 is the termination of clone elimination. Clone contour rounds up and relaxes at -32 min and is followed by wound healing. Inset on the right shows E-cad accumulation at tricellular junctions during wound healing. Scale bar= 10 μ m.

d: Evolution of the clone area shown in **c**. The grey zone corresponds to the relaxation phase and is followed by wound healing. The lines corresponds to the timing of the images shown in **c**. Inset shows increased of clone solidity (area/convex area) during the relaxation and wound healing phases (grey zone).

e: Snapshots of clones of different sizes expressing optoDronc upon blue light exposure. Note the transient relaxation at 41 min for 5 cells cluster. Time 0 is the onset of blue light exposure. Scale bars= 10 μ m.

f: Quantification of the proportion of normal and aberrant extrusions (extrusions followed by transient relaxation or E-cad accumulation at vertices) and/or transient hole (large relaxation and E-cad accumulation at vertices) observed for clone disappearance of different sizes and topologies (see schematic below). n=number of clones. Error bars are 95% confidence interval.

g: Injection of far red Dextran 10,000 MW in pupal notum. Bottom shows a transverse view of Dextran signal in the pupae (x- antero-posterior, Z- apical-basal). Schematic showing the localisation of Dextran according to the epithelium (AJs: adherens junctions, SJs: septate junctions). Note that septate junctions are located basally to adherens junctions.

h: Local projections of optoDronc clones composed of one to several cells in lines after Dextran injection (bottom). Time 0 is the end of clone elimination. No dextran appears at the level of adherens junctions during clone elimination. Scale bar= 10 μ m.

i: Local projections of an optoDronc clone composed of four cells in cluster after Dextran injection (bottom). Time 0 is the end of clone elimination. During the relaxation phase (-35min) dextran appears at the level of adherens junctions (white squares). Scale bar= 10 μ m.

j: Quantification of the far red Dextran signal during optoDronc clone elimination (in line, black, or in clusters of 3-4 cells, red). The curves are the median +/- s.e.m.. Top inset shows the average clone area during their elimination (note that the elimination is overall slower for clusters, red curve).

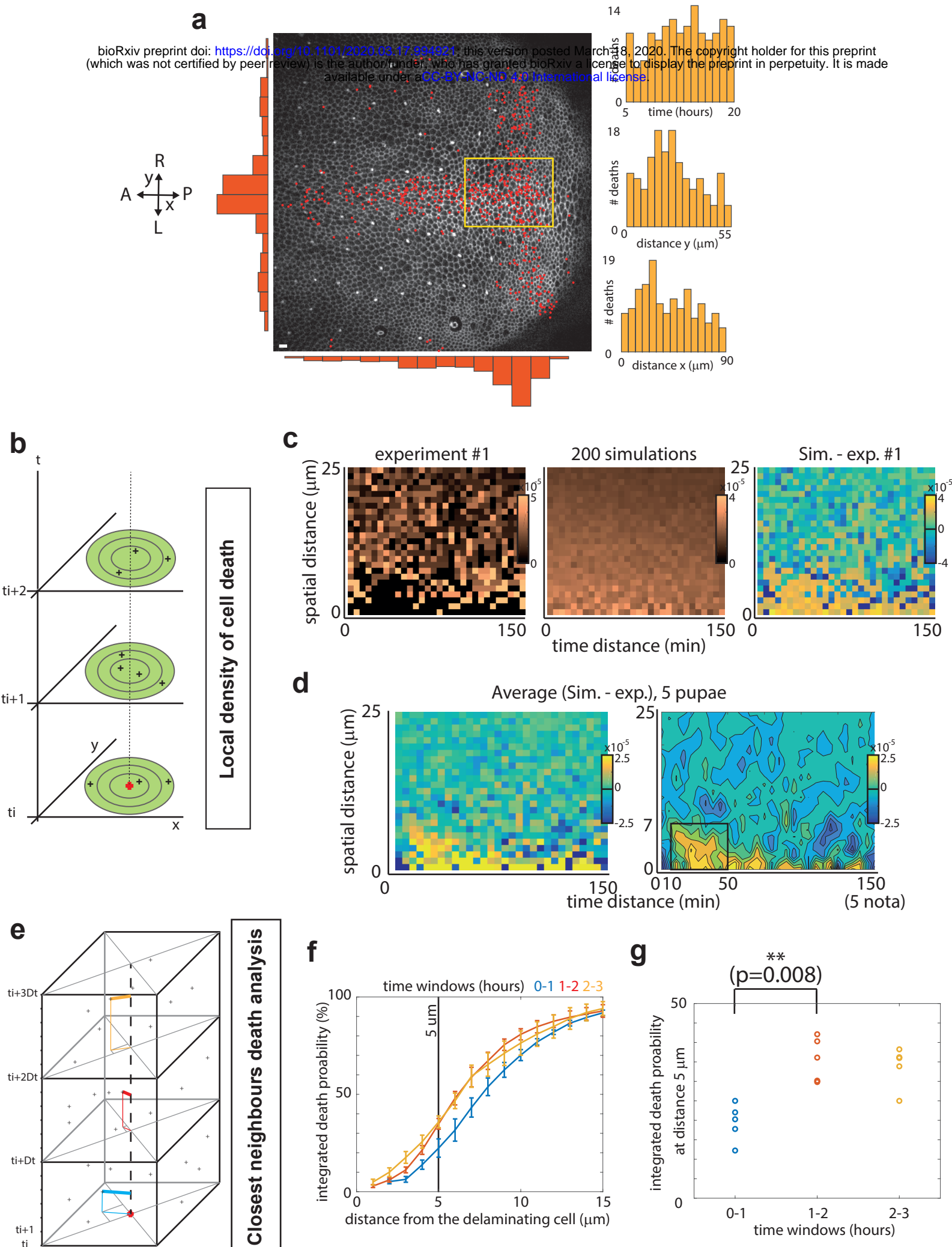


Figure 2: There is a transient and local refractory phase for cell elimination following each cell death.

a: Snapshot of a local projection of a pupal notum expressing E-cad-GFP. Red dots are showing every cell extrusion occurring over 21 hours. A: Anterior, P: Posterior, L: Left, R: Right. Scale bar= 10 μ m. Orange histograms show the spatial distribution of cell death over left-right axis (left) or along AP axis (bottom). Right histograms show the temporal distribution of cell death (top) and its spatial distribution (middle and bottom) in the yellow rectangle region (used for further analysis). **b:** Schematic explaining the rationale of the measurement of death distribution. For each death event, the density of cell death in a disc at a given distance is calculated for each time point. **c:** Local cell death density (yellow: high density) at different distances from a dying cell (y axis) for different times (x axis, minutes) for one movie. The middle map shows the average map obtained for 200 simulations assuming independent events with the same proportion of dying cells. The right map shows the difference between the simulated distribution and the experimental distribution (death at short distances are under-represented in the experiment). **d:** Average of the difference between experimental maps and the corresponding simulated maps (see **Figure S2** for details, 5 movies). The right map is obtained after median filtering. Note the bottom left yellow domain with lower probability of cell death compared to simulations (black square, 7 μ m~one cell diameter, and from ~ 10 to 60min). **e:** Analysis of cell death distribution through a closest neighbour approach. Time is subdivided in arbitrary windows (here 1 hour, starting from t=20 minutes) and for each time window the closest cell death is found. **f:** Cumulative plots of the probability to find the closest death at a given distance for different time windows (20min to 1h20, 1h20 to 2h20, 2h20 to 3h20). The curves are averages of 5 movies, error bars are s.e.m.. Note that only the blue curve detaches from the others, representing what happens 20 to 80 minutes after cell death. **g:** Details of the values obtained for a distance of 5 μ m (~ 1 cell distance) for each time window (one dot = one pupa). There is a two-folds reduction of the probability to have cell death occurring on the first hour after cell elimination from 0 to 5 μ m.

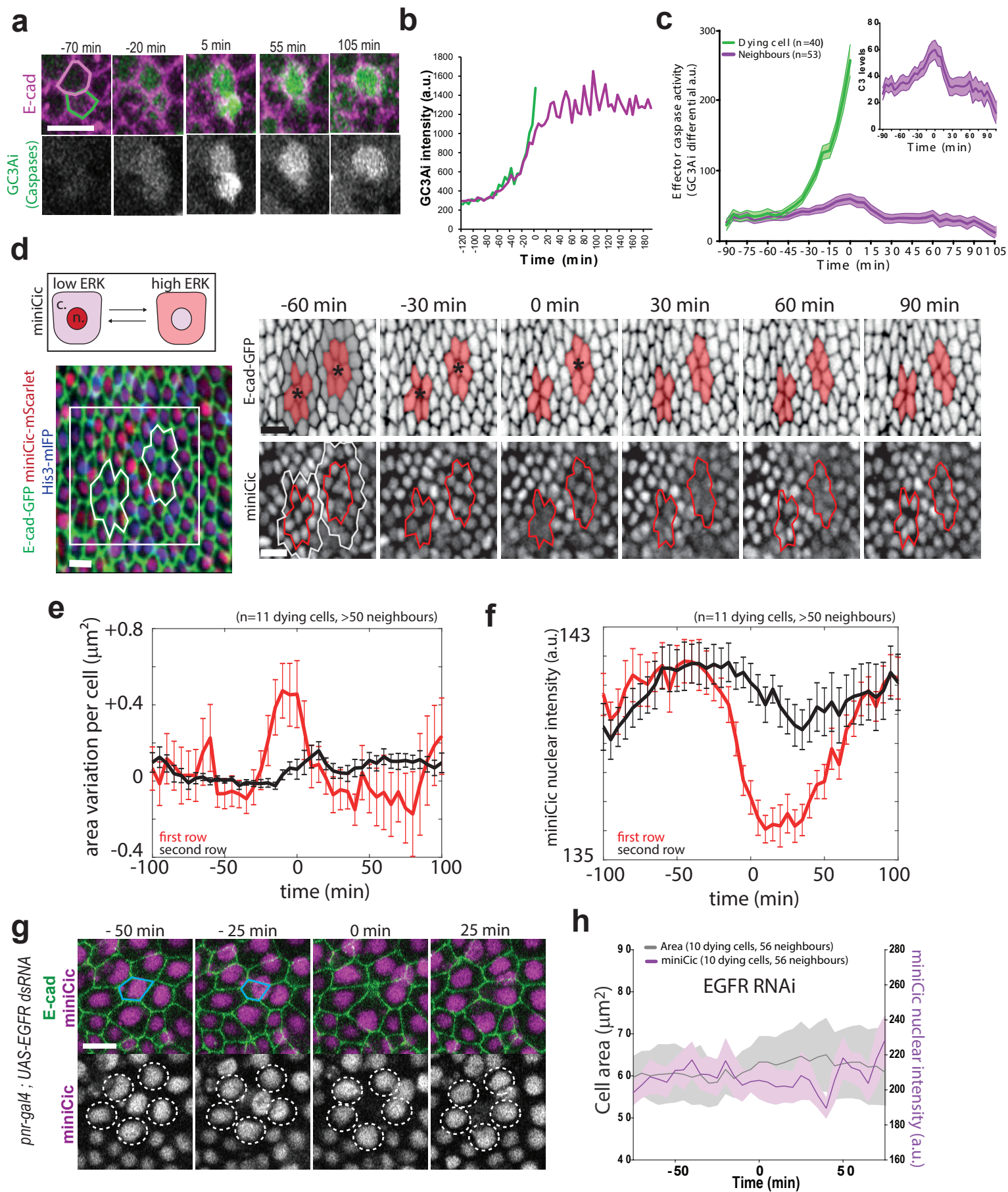


Figure 3: Transient ERK activation in cells neighbouring an extruding cell

a: Snapshots of local projections of a pair of cells in the pupal notum tagged with E-cad-tdTomato and expressing the effector caspase sensor GC3Ai (green). Time 0 is the termination of extrusion of the bottom cell (green contour). Scale bar=10 μ m. **b:** Intensity of GC3Ai in the eliminated cell (green) and its neighbour (purple). Note that GC3Ai signal plateaus in the neighbour after the first cell is eliminated. **c:** Averaged GC3Ai differential (a proxy of effector caspase activity, see **Methods**) for dying cells (green) and its neighbours (purple). Neighbours undergo transient caspase activation followed by reversion. Time 0 is the termination of the first cell extrusion. Light coloured areas show s.e.m. The top inset shows the purple curve with higher magnification. **d:** top: schematic showing the localisation of miniCic (n. : nucleus, c.: cytoplasm) upon modulation of ERK activity. Bottom: Snapshot of the posterior region of the pupal notum with two dying cells (red: miniCic-mScarlet, green: E-cad-GFP, blue: His3-mIFP). Right: snapshots of two dying cells (black stars) showing E-cad signal (inverted colour, top) and miniCic (bottom). Orange zones (red line for miniCic) are the first row of neighbouring cells, grey zones (white line for miniCic) mark the second row. Scale bars=10 μ m. **e:** Averaged cell apical area variation in the first row (red) and second row (black) of cells neighbouring an extruding cell. Time 0 is the termination of extrusion. Error bars are s.e.m.. **f:** Averaged nuclear miniCic intensity in the first row (red) and second row of cells (black). Error bars are s.e.m.. **g:** Snapshots of a *pnr-gal4 ; UAS-EGFRdsRNA* pupae (local projections) expressing E-cad-GFP, miniCic-mScarlet and His3-mIFP (not shown). The blue line shows a dying cell. The white dotted circles show miniCic signal in the nuclei of the neighbouring cells. Scale bar=10 μ m. **h:** Averaged nuclear miniCic intensity (purple) and cell apical area (black) in EGFR depleted nota in the cells neighbouring an extruding cell (Time 0 is the termination of extrusion). Light areas are s.e.m..

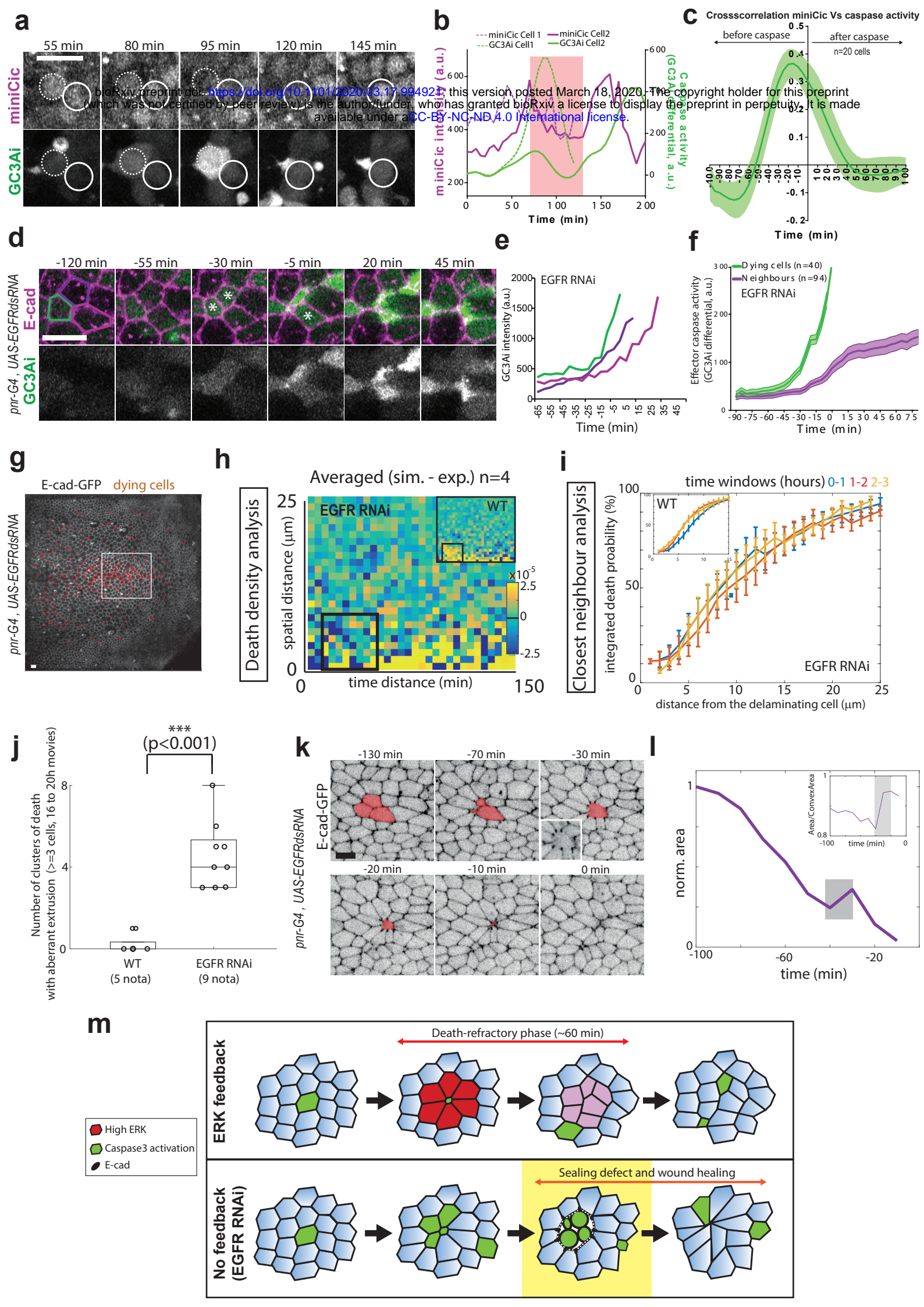


Figure 4: ERK pulses are required for caspase reversion and to prevent clusters of cell elimination

a: Snapshots of local projections of a pupal notum expressing miniCic and GC3Ai. White dotted circles show the first dying cell, white circles show one of its neighbours dying later. Time is in agreement with the curves shown in **b**. **b:** Nuclear miniCic signal (magenta) and GC3Ai differential (green, caspase activity) in the first dying cell (dotted lines) and its neighbours (plain lines) shown in **a**. The red region shows the pulse of ERK in the neighbours and the subsequent transient reversion of caspase activity. **c:** Averaged normalised cross-correlation between miniCic nuclear signal and caspase activity (GC3Ai differential). Peak at -15 min indicates a 15 minutes delay between ERK activation and caspase reversion. **d:** Snapshots of a local projection of a *pnr-gal4*, *UAS-EGFRdsRNA* pupal notum expressing E-cad-tdTomato and GC3Ai. The white stars show several neighbouring cells dying. Green, light and dark purple cell contours correspond to the curves shown in **e**. Scale bar=10 μ m. **e:** GC3Ai intensity in the three cells marked in **d**. Time 0 is the termination of extrusion of the first dying cell (green contour). Note that there is no inflexion of GC3Ai signal in the neighbours. **f:** Averaged GC3Ai differential signal (caspase activity) in the dying cell (green) and its neighbours (purple) upon depletion of EGFR in the notum. Light areas are s.e.m.. Time 0 is the termination of extrusion of the first dying cell. On average, caspase activity is maintained in the neighbouring cells (differential >0, compare with **Figure 3b,c**). **g:** Local projection of a E-cad-GFP pupae depleted for EGFR (*pnr-gal4*, *UAS-EGFR dsRNA*). Red dots show all the dying cells over the course of the movie (21 hours). Scale bar=10 μ m. The white rectangle show the region of analysis used for **h** and **i**. **h:** Averaged differences between the experimental distribution of cell death density in four EGFR depleted pupae and the simulated distribution (assuming independent events). The inset shows the same analysis for WT pupae (see **Figure 2d**). Note the absence of yellow in the bottom left corner compared to the WT (no reduction of cell death density in EGFR depleted pupae for 10-60 min, <7 μ m). **i:** Closest neighbour analysis of cell death distribution in EGFR depleted pupae (see **Figure 2 e-g**). Integrated death probability for

different time windows after cell elimination (20min-1hour 20, 1h20-2h20, 2h20-3h20) at different distances from the dying cells. While the first hour distribution was different in the WT (see top left inset, blue curve), there is no apparent differences upon EGFR depletion. **j**: Number of occurrences of clustered elimination (≥ 3 cells) followed by aberrant extrusion per movie (16 to 20 hours) in the WT pupae (5 nota) and upon depletion of EGFR (*pnr-gal4, UAS-EGFR dsRNA*, 9 pupae). **k**: Snapshots of E-cad-GFP local projection in a EGFR depleted pupae showing concomitant elimination of three cells (orange area) and an aberrant extrusion (relaxation at -30 and wound healing figure with E-cad accumulation at vertices, bottom left inset, compare with **Figure 1 c,d**). Time 0 is the termination of cell elimination. **l**: Evolution of the clone area shown in **k**. The grey zone corresponds to the relaxation phase and is followed by wound healing. Inset shows increased of clone solidity (area/convex area) during the relaxation and wound healing phases. **m**: Schematic of the local ERK feedback (red) and its impact on the distribution of cell elimination (green cells: caspase activation). Upon EGFR depletion, simultaneous caspase activation and cell elimination can occur, which leads to aberrant extrusion and transient loss of sealing (phase outlined in yellow, white area between green aggregates) followed by wound healing.

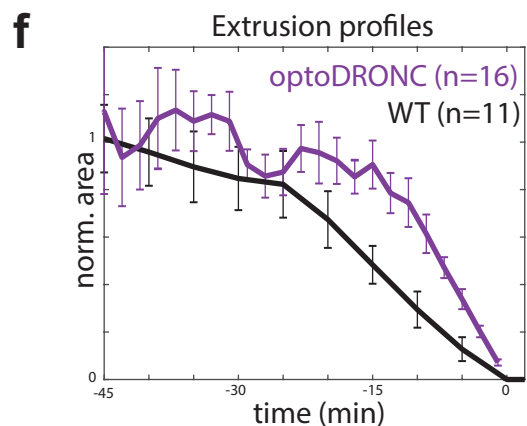
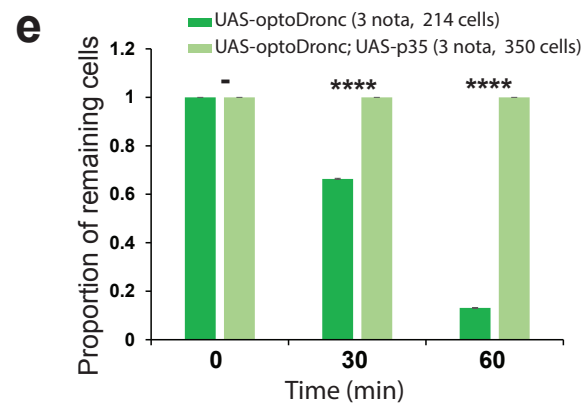
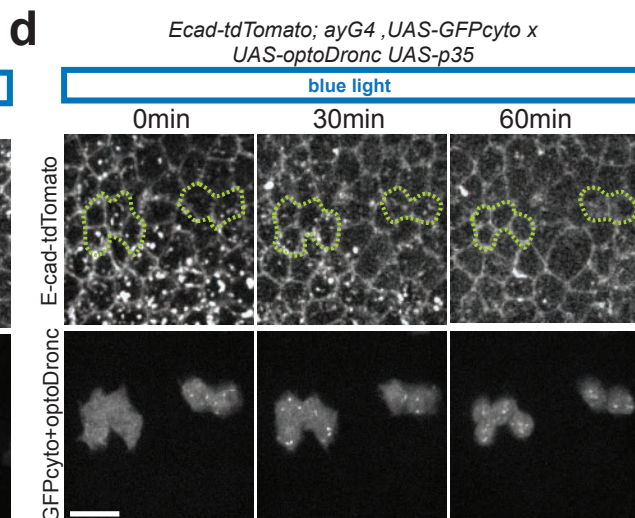
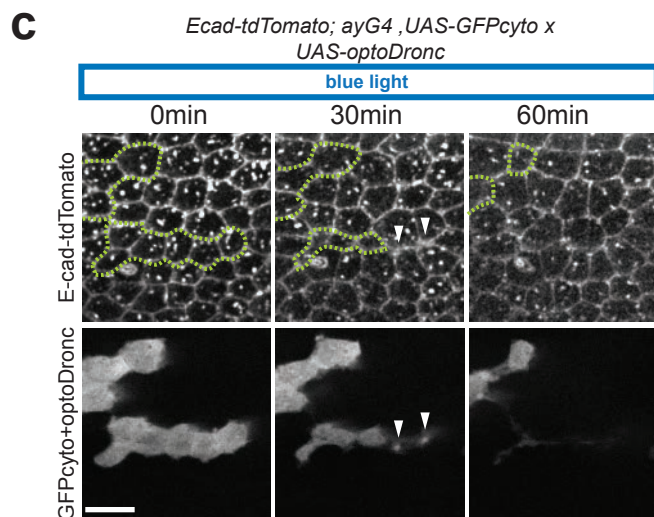
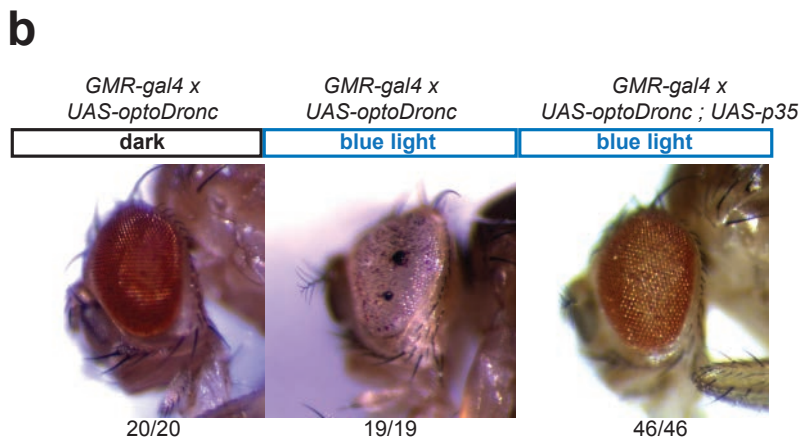
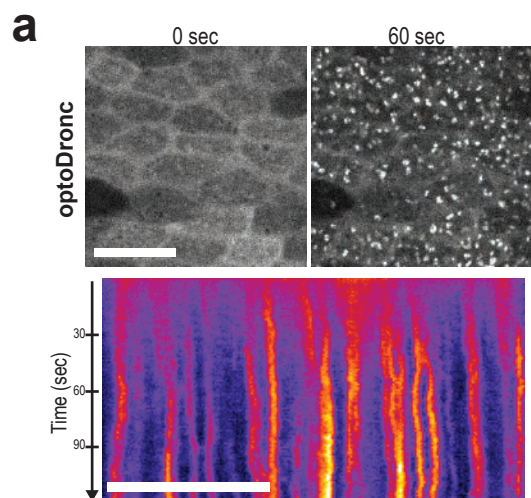


Figure S1: optoDronc triggers cell extrusion through effector caspase activation

a: Rapid clustering of UAS-optoDronc (GFP fusion) upon blue light exposure (single plane movie, 1 frame/sec). Scale bar= 10 μ m. Bottom: kymograph of optoDronc-GFP signal (clusters already appear after 20 sec) **b:** GMR-gal4 adult *Drosophila* eyes expressing UAS-optoDronc from flies raised in a blue light chamber (left), in the dark (middle) or with p35 overexpression (effector caspase inhibitor) in the light chamber. N are numbers of females. **c,d:** Snapshots of pupal nota (local projection) expressing *UAS-optoDronc* (**c**) or *UAS-optoDronc* and *UAS-p35* (**d**) in clones (bottom, UAS-GFP and optoDronc-GFP in the same channel) and E-cad-tdTomato. Green lines show clone contours. White arrowheads show extruding cells. Scale bars=10 μ m. **e:** Proportion of clonal cells remaining in the epithelium upon blue light exposure expressing *UAS-optoDronc* (green) or *UAS-optoDronc; UAS-p35* (light green). Error bars are 95% confidence interval, -= non-significant, ****= $p < 10^{-4}$. **f:** Averaged and normalised cell apical area during spontaneous extrusion (black curve, WT movie, frame rate 5min) or upon induction of extrusion through light activation of optoDronc in single cell clones (purple curve). Curves are aligned at time 0 min (cell apical area = 0). Error bars are s.e.m.. Note that optoDronc-triggered extrusion is slightly faster than WT extrusion but globally similar.

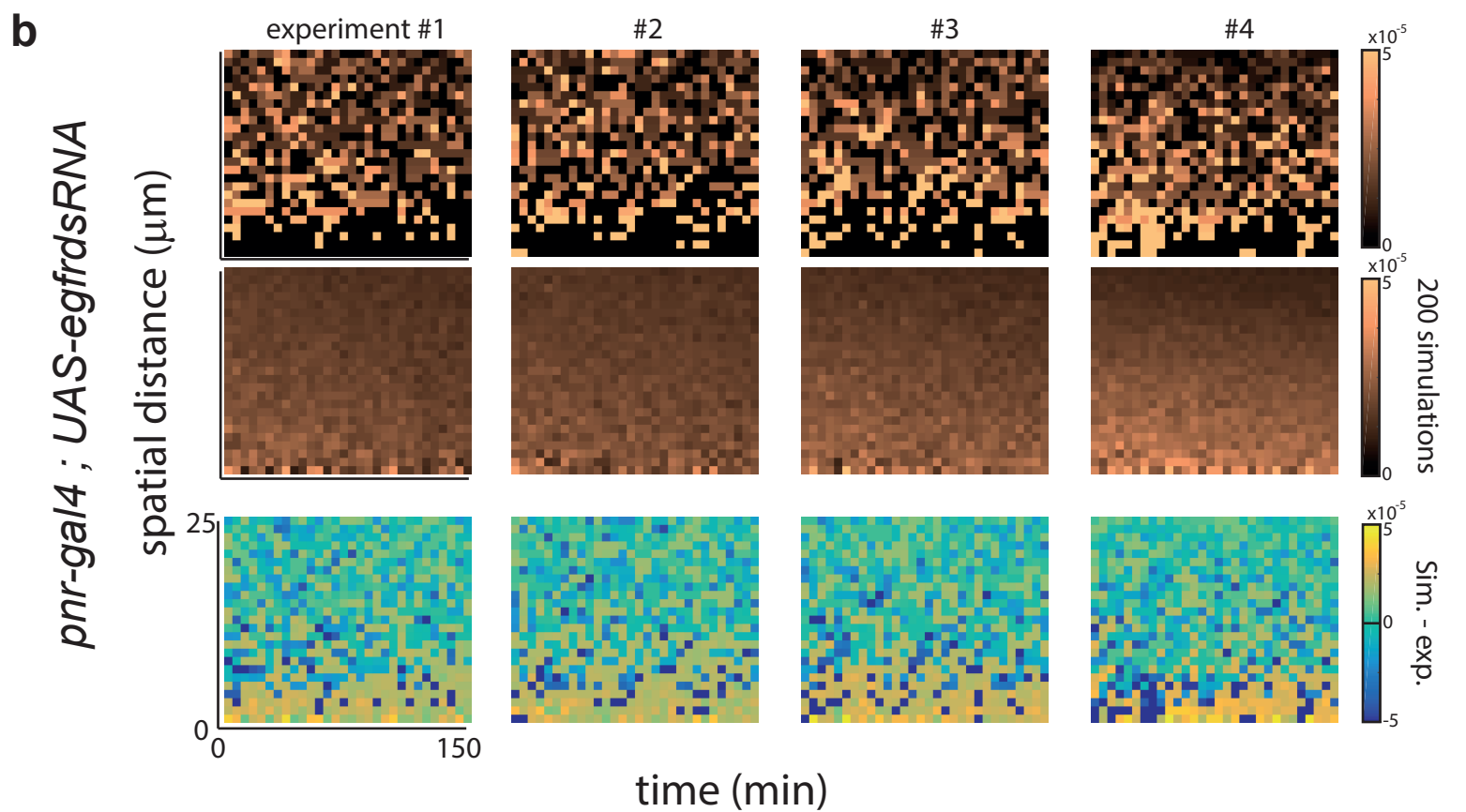
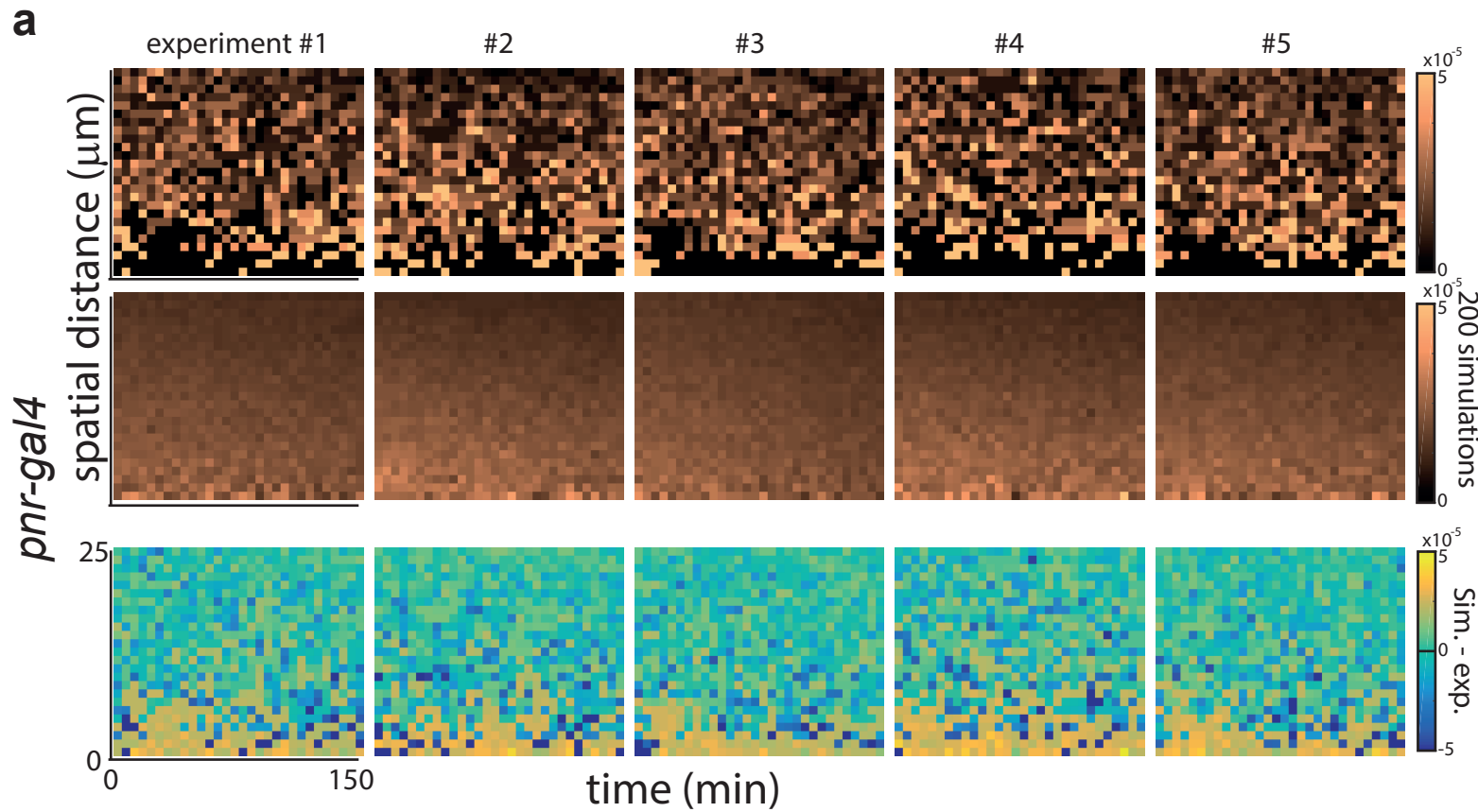


Figure S2: Distribution of cell death in control *nota* and upon depletion of EGFR

a,b: Maps of the local death density near each dying cells at different times (see **Figure 2b-d**) for control pupae (**a**, *pnr-gal4*) or upon depletion of EGFR (**b**, *pnr-gal4; UAS-EGFR dsRNA*). Top: experimental distribution (one map = one pupa), y: spatial distance in μm , x: time distance in minutes. Middle: simulations of the death distribution for the corresponding experiment assuming a Poisson process (average of 200 simulations). Bottom: Difference between experiment and simulation distributions (yellow= low proportion of cell death compared to simulations).

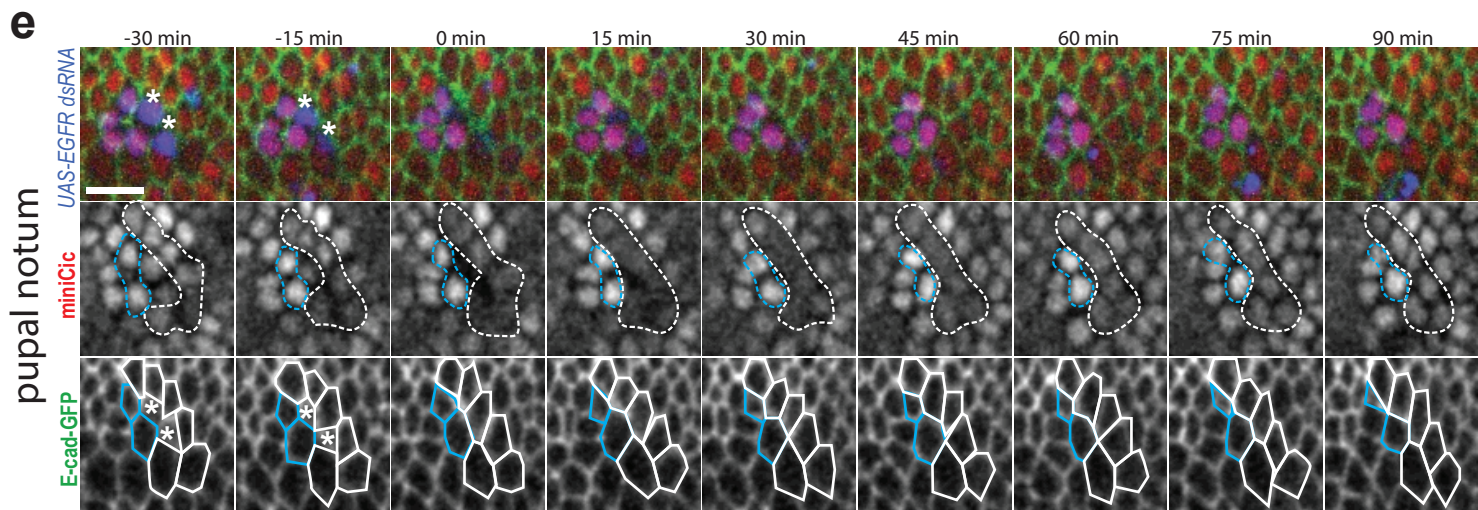
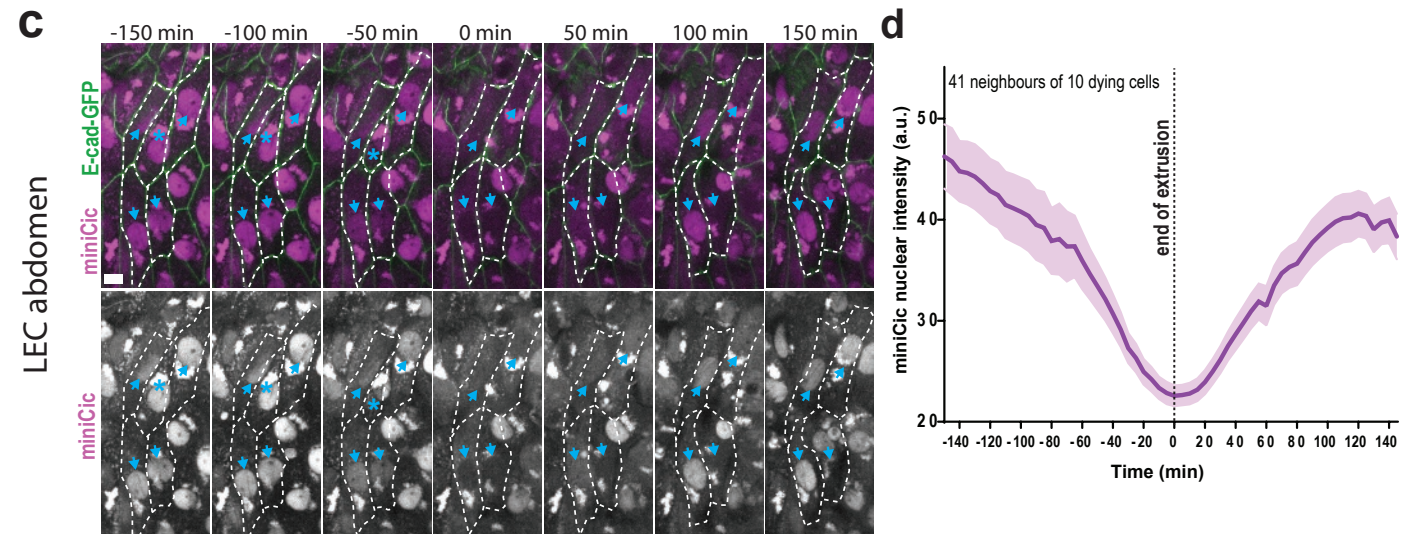
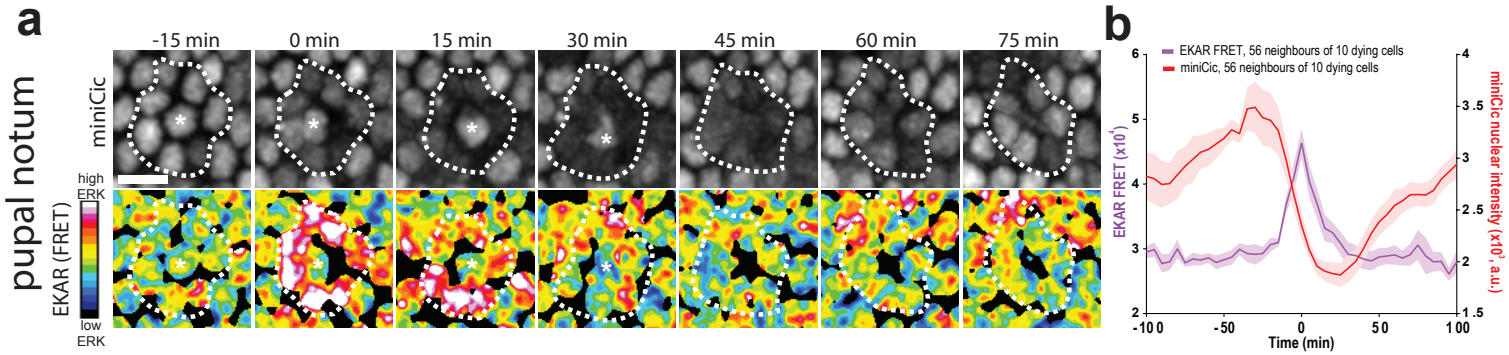


Figure S3: ERK pulses are also present in the abdomen and require EGFR cell-autonomously.

a: Snapshots of local projections of a pupal notum expressing miniCic (top, grey) and a FRET sensor of ERK (EKAR, bottom). Red signal: high ERK, blue signal: low ERK. The white star marks a dying cell. The dotted lines show the miniCic and the FRET signal in the neighbouring cells. Scale bar=10 μ m. **b:** Averaged nuclear miniCic intensity (red) and FRET signal (purple) in the neighbours of dying cells. The curves were aligned on the peak of the FRET signal. Light areas are s.e.m.. Note that miniCic nuclear exclusion correlates well with the pulses of FRET activity (although there is a delay in the relocation of miniCic to the nucleus). **c:** Snapshots of local projections in the larval accessory cells (LECs) of the pupal abdomen expressing E-cad-GFP and miniCic. Blue stars show an extruding cell, blue arrows show the nuclei of neighbouring cells (which lose transiently miniCic signal). Dotted lines show cell contours. Scale bar=10 μ m. **d:** Averaged nuclear miniCic signal in the LECs neighbouring extruding cells (Time 0 is the termination of extrusion). Light areas are s.e.m.. **e:** Snapshots of a local projection of a pupal notum with *UAS-egfr dsRNA* clones (blue, UAS-His3-mIFP) expressing E-cad-GFP and miniCic. White stars show two *egfr* RNAi cells extruding. Blue lines show the contour and the nuclei of two *egfr* RNAi cells neighbouring the dying cells, white lines show the contours and nuclei of WT cells neighbouring the dying cells. Note that dying EGFR depleted cells can still activate ERK in the WT neighbours (loss of nuclear miniCic) but ERK does not get activated in EGFR depleted cells. Scale bar=10 μ m.

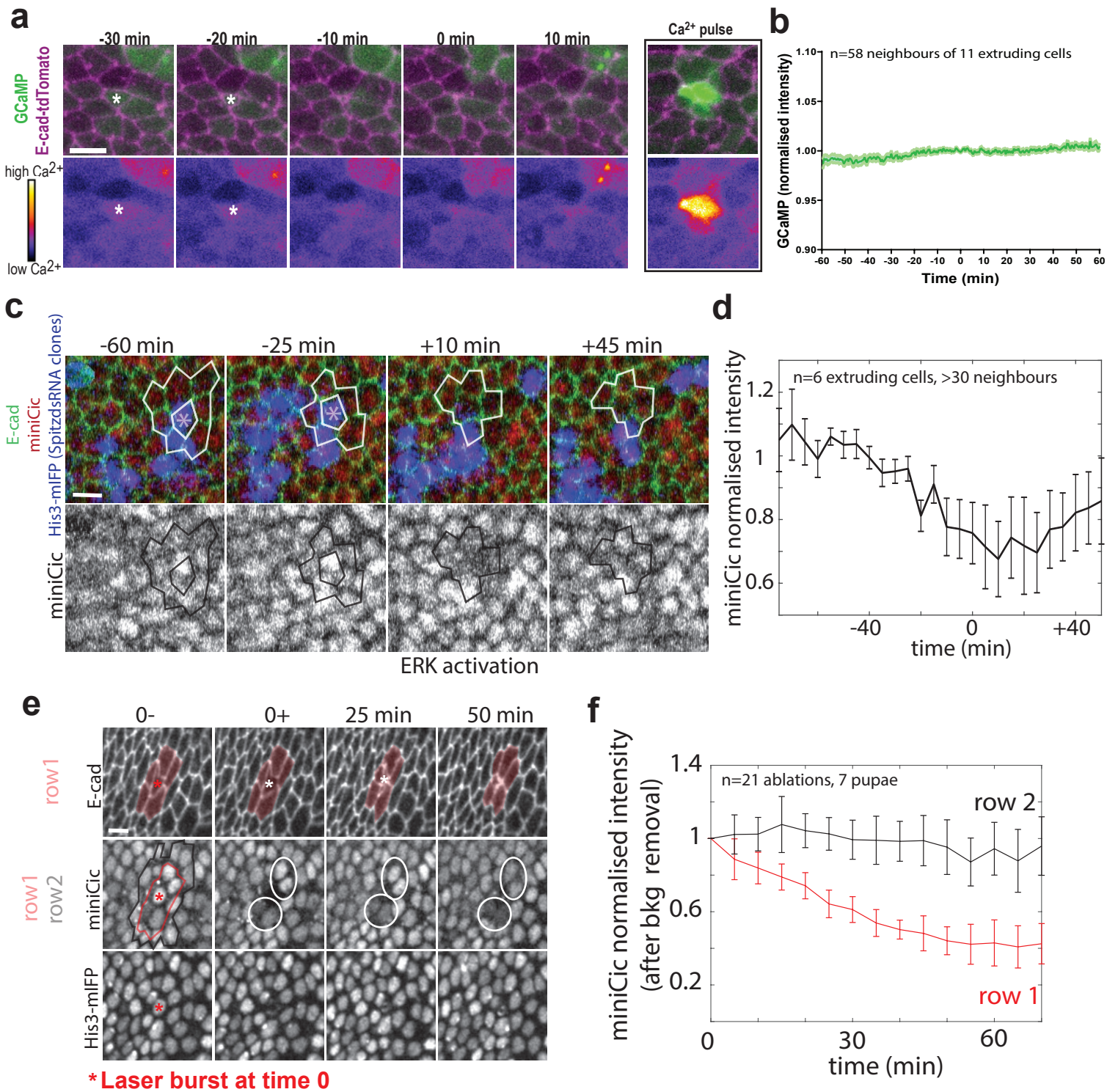


Figure S4: ERK pulses do not correlate with Ca^{2+} pulses, do not require Spitz expression in the dying cells, and can be mimicked by wound healing-induced stretching.

a: Snapshots of local projections of a pupal notum expressing the Calcium sensor GCaMP (pseudo colour) and E-cad-tdTomato. The white stars show a dying cell. There is no visible change of Ca^{2+} activity in the neighbours or in the dying cell. The right inset show an example of rare spontaneous pulse of Ca^{2+} (one or two per movie, not correlation with cell death). Scale bar= $10\mu\text{m}$. **b:** Averaged and normalised GCaMP signal in cells neighbouring extruding cells (Time 0, termination of extrusion). Light area is s.e.m.. **c:** Snapshots of a local projection of a pupal notum with *UAS-spitz dsRNA* clones (blue, UAS-His3-mIFP) expressing E-cad-GFP and miniCic. The stars show a dying Spitz RNAi cell, white lines show the contour of the neighbours. Scale bar= $10\mu\text{m}$. **d:** Averaged and normalised miniCic nuclear intensity in cells neighbouring Spitz RNAi extruding cells (Time 0, termination of extrusion). Error bars are s.e.m.. **e:** Snapshots of local projection of a pupae expressing E-cad-GFP, miniCic and His3-mIFP. The cell marked with a red star is laser ablated at time 0. Pink line/area show the first neighbours, black line the second row of neighbours. The white circles show miniCic signal in the direct neighbours of the laser ablated cell. Scale bar= $10\mu\text{m}$. **f:** Averaged and normalised nuclear miniCic signal (after background removal, acquisition on a spinning disc) in the first row (red) and second row (black) of cells neighbouring the laser ablated cells. Time 0 is the ablation time.

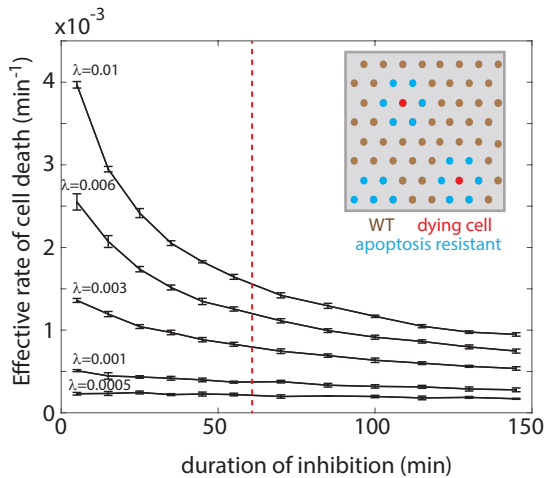
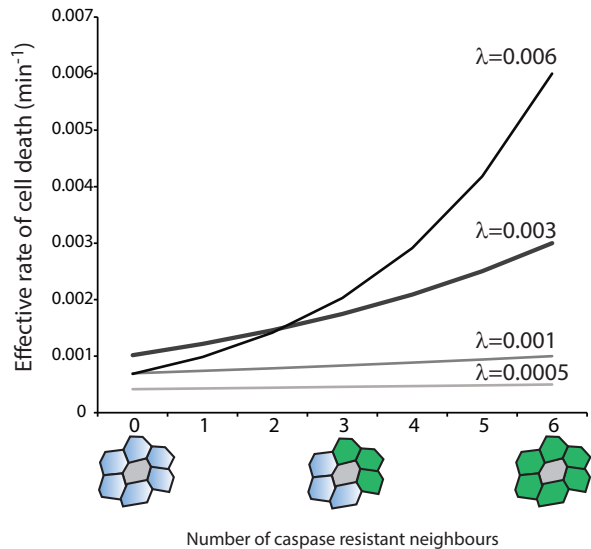
a**b**

Figure S5: ERK pulses can modulate significantly the rate of cell death and could recapitulate features of cell competition

a: 2D simulation of the distribution of cell death assuming a local refractory phase of various times (see **Methods**). λ are intrinsic rates of cell elimination (in absence of feedbacks). Note that the curves start at $T=5$ minutes. For a refractory phase of 60 minutes (red curve, as estimated experimentally), the curve showing a rate of cell elimination similar to the one measured in the posterior region of the pupal notum ($\sim 0.001/\text{minute}$) corresponds to an intrinsic rate of cell death $\lambda=0.03$. **b:** Estimation of the probability of cell death in a cell (grey) neighbouring various number of caspase resistant cells (0 to 6, green cells). See **Methods**. λ is the intrinsic rate of cell elimination (number of cell death per minute without feedback). The thick grey curve ($\lambda=0.03$) is the one closest to the putative intrinsic rate of elimination estimated from **Figure S5a**. There is close to a three folds increase of the rate of cell elimination when the cell is surrounded by six caspase resistant neighbours. Therefore, in a region with a high rate of cell elimination, clones resistant for apoptosis will increase the rate of neighbouring cell elimination (similar to a cell competition scenario).

Video legends

Video S1: Induction of clone elimination by optoDronc is effector caspase-dependent

Local projections of pupal nota expressing E-cad-tdTomato (green) and optoDronc (magenta, left) or optoDronc and p35 (magenta, right) in clones. Blue light exposure starts at the onset of the movies. Scale bars=10 μ m.

Video S2: Induction of extrusion by optoDronc in different clone topologies

Local projections of pupal nota expressing E-cad-tdTomato (green) and optoDronc (magenta) in clones of various sizes (one cell, two cells, three cells in row, three cells in cluster, more than four cells in cluster). Blue light exposure starts at the onset of the movies. Scale bars=10 μ m.

Video S3: optoDronc clone elimination and Dextran diffusion

Local projections of pupal nota expressing E-cad-tdTomato (green, middle) and optoDronc (magenta) in clones upon injection of far red Dextran (grey levels, same plane as E-cad, right). Top part shows a line of four cells, bottom a cluster of four cells with aberrant extrusion. Blue light exposure starts at the onset of the movies. Scale bars=10 μ m.

Video S4: Cell extrusion localisation in a WT notum

Local projection of a pupal notum marked with E-cad-GFP showing every cell extrusion (coloured circles). Anterior: left, Posterior: right. Circles appear at the termination of extrusion (orange) and stay for nine frames (progressively becoming blue). Scale bar=10 μ m.

Video S5: Reversion of caspase activity in a cell neighbouring an extruding cell

Local projection of a pupal notum expressing GC3Ai (green and right, effector caspase activity) and E-cad-tdTomato (magenta). The bottom cell dies, while GC3Ai signal stop increasing in the top cell which remains in the tissue. Scale bar=10 μ m.

Video S6: Transient activation of ERK in cells neighbouring extruding cells

Local projection of a pupal notum expressing miniCic-mScarlet (magenta, bottom right, ERK sensor), E-cad-GFP (green, top right) and His3-mIFP (grey, bottom left). Cells marked in cyan are extruding. The white lines show the nuclei of the direct neighbouring cells (transient loss of nuclear miniCic= ERK activation). Scale bar=10 μ m.

Video S7: Transient ERK activation is also visible with a FRET sensor

Local projection of a pupal notum expressing miniCic-mScarlet (grey, left), and EKARNls (ERK FRET sensor, FRET ratio in pseudocolour, red=activation, blue=inhibition). The green circles show a dying cell. Note the transient loss of nuclear miniCic in the direct neighbours and the transient burst of FRET signal. Scale bar=10 μ m.

Video S8: There is no visible Ca²⁺ pulses near extruding cells

Local projection of a pupal notum expressing GCaMP (green, right), and E-cad-tdTomato (magenta). The cyan contours show an extruding cell. Scale bar=10 μ m.

Video S9: Spitz is not required in the dying cell to activate ERK in the neighbours

Local projection of a pupal notum expressing miniCic-mScarlet (magenta, bottom right, ERK sensor), E-cad-GFP (green, top right) and His3-mIFP in clones expressing Spitz-dsRNA (grey, bottom left). The cell in cyan is a Spitz RNAi cell dying. The white circles show the nuclei of direct neighbouring WT cells (transient loss of nuclear miniCic = ERK activation). Scale bar=10 μ m.

Video S10: Activation of ERK driven by single cell laser ablation

Local projection of a pupal notum expressing miniCic-mScarlet (magenta, bottom right, ERK sensor), E-cad-GFP (green, top right) and His3-mIFP (grey, bottom left). The cell in cyan is ablated by a UV pulsed laser at time 0. The white circles show the nuclei of direct neighbouring cells (transient loss of nuclear miniCic = ERK activation). Scale bar=10 μ m.

Video S11: EGFR is required for extrusion-induced ERK activation

Local projection of a pupal notum depleted for EGFR (*pnr-gal4, UAS-egfrdsRNA*) expressing miniCic-mScarlet (red, bottom left, ERK sensor), E-cad-GFP (green, top right)

and His3-mIFP (blue, bottom right). White contours show the dying cell. The white circles show the nuclei of direct neighbouring cells (no change of nuclear miniCic, no ERK activation). Scale bar=10 μ m.

Video S12: ERK is also activated by cell extrusion in the pupal abdomen

Local projection of larval accessory cells in the pupal abdomen expressing miniCic-mScarlet (magenta, grey on the right, ERK sensor) and E-cad-GFP (green). The red contours show the dying cell. The blue contours show the direct neighbours. Scale bar=10 μ m.

Video S13: ERK pulses precede effector caspase inhibition

Local projection of a pupal notum expressing GC3Ai (green and right, effector caspase activity) and miniCic (magenta, middle). Green circles track the nucleus of the first dying cell. Purple circles track the nucleus of a neighbour undergoing transient caspase inhibition (slow-down of GC3Ai signal increase). Scale bar=10 μ m.

Video S14: EGFR depletion abolishes caspase reversions

Local projection of a pupal notum depleted for EGFR (*pnr-gal4*, *UAS-egfrdsRNA*) expressing GC3Ai (green and right, effector caspase activity) and E-cad-tdTomato (magenta). Coloured contours show neighbouring cells activating caspase. Scale bar=10 μ m.

Video S15: Cell extrusion localisation in a EGFR RNAi notum

Local projection of a pupal notum depleted for EGFR (*pnr-gal4*, *UAS-egfrdsRNA*) marked with E-cad-GFP showing every cell extrusion (coloured circles). Anterior: left, Posterior: right. Circles appear at the termination of extrusion (orange) and stay for nine frames (progressively becoming blue). Scale bar=10 μ m.

Video S16: Clusters of cell elimination and aberrant extrusions appear upon EGFR depletion

Local projection from different pupal nota depleted for EGFR (*pnr-gal4*, *UAS-egfrdsRNA*) marked with E-cad-GFP showing four examples of clusters of cell extrusion (cyan, more

than four cells) followed by aberrant extrusions (relaxation, wound healing and E-cad accumulation at vertices). Scale bar=10 μ m.